KATHOLIEKE UNIVERSITEIT LEUVEN

FACULTEIT FARMACEUTISCHE WETENSCHAPPEN

INTERACTION OF ACYCLIC NUCLEOSIDE PHOSPHONATES WITH THE TWO 6-OXOPURINE PHOSPHORIBOSYLTRANSFERASE PURINE SALVAGE ENZYMES FROM *E. coli*

Rega Instituut
Afdeling Virologie en Chemotherapie
Prof. Dr. L. Naesens

The School of Chemistry and Molecular Biosciences
The University of Queensland, Brisbane, 4072 QLD, Australia
Prof. Dr. L. Guddat
Begeleiding: Prof. J. de Jersey, Prof. I. Brereton, Dr. D. Keough

Masterproef ingediend
tot het behalen
van het Diploma
van Master in de
Geneesmiddelenontwikkeling
door **Harmen JANS**

Leuven 2010-2011

KATHOLIEKE UNIVERSITEIT LEUVEN

FACULTEIT FARMACEUTISCHE WETENSCHAPPEN

INTERACTION OF ACYCLIC NUCLEOSIDE PHOSPHONATES WITH THE TWO 6-OXOPURINE PHOSPHORIBOSYLTRANSFERASE PURINE SALVAGE ENZYMES FROM *E. coli*

Rega Instituut
Afdeling Virologie en Chemotherapie
Prof. Dr. L. Naesens

The School of Chemistry and Molecular Biosciences
The University of Queensland, Brisbane, 4072 QLD, Australia
Prof. Dr. L. Guddat
Begeleiding: Prof. J. de Jersey, Prof. I. Brereton, Dr. D. Keough

Masterproef ingediend
tot het behalen
van het Diploma
van Master in de
Geneesmiddelenontwikkeling
door **Harmen JANS**

Leuven 2010-2011

Acknowledgements

At this place I would like to thank all those who have contributed to the realization of my thesis. First of all, I want to thank Prof. Lieve Naesens and Prof. Luke Guddat for making it possible for me to do my research work in Brisbane. This thesis would not have been possible without them. Prof. Guddat I thank greatly for welcoming me in his lab and for his expertise during my experiments. Many thanks go to Dr. Dianne Keough for her everyday help and advice and the endless correction of this work. I would like to show my gratitude to Prof. Ian Brereton and Dr. Greg Pierens for their help and suggestions during the NMR experiments. Special thanks go to Prof. John de Jersey. His enthusiasm has deeply stimulated my interest in this area of scientific research. I would also like to thank the people in the lab for the friendly atmosphere.

I want to thank Grace Hyeree, Chelsea Kahn, Falah Alsharari, Beccy Saleeb, Sam Winterflood, Sam Xinis and many others for making my stay in Brisbane a memorable experience. Furthermore, I specially want to thank my girlfriend Sofie for her infinite patience with me, the many hours of skype, her ability to make me laugh and the unforgettable trip around Australia.

And last but not least, I owe my deepest gratitude to my parents and brothers, Mathias and Lennart. My Australian adventure would have never been possible without their endless support, encouragement, trust and love.

TABLE OF CONTENTS

MASTER'S THESIS PART 2: RESEARCH PROPOSAL

LIST OF ABBREVIATIONS

A_{600}	absorbance at 600 nm
ADA	adenosine deaminase
AMP	adenosine monophosphate
ANP	acyclic nucleoside phosphonate
APRT	adenine phosphoribosyltransferase
BSA	bovine serum albumine
cfu/ml	colony-forming units per milliliter
Δε	extinction coefficient
DMEM	Dulbecco's minimal essential medium
DR3876	(*R*)-(2-(3-(2-amino-6-oxo-1*H*-purin-9(6*H*)-yl)pyrrolidin-1-yl)-2oxoethyl)-phosphonic acid
DTT	dithiothreitol
GMP	guanosine 5'-monophosphate
HGPRT	hypoxanthine-guanine phosphoribosyltransferase
HGXPRT	hypoxanthine-guanine-xanthine phosphoribosyltransferase
hHGPRT	human hypoxanthine-guanine phosphoribosyltransferase
HPMPA	9-[3-hydroxy-2-(phosphonomethoxy)propyl] adenine
HPP	7-hydroxy [4,3-d] pyrazolo pyrimidine
HPRT	hypoxanthine phosphoribosyltransferase
H_x	hypoxanthine
IC_{50}	concentration required to inhibit parasite growth or cell proliferation by 50%
ImmGP	immucillinGP
ImmucillinGP	(1S)-1-(9-deazaguanin-9-yl)-1,4-dideoxy-1,4-imino-D-ribitol 5-phosphate
IMP	inosine 5'-monophosphate
LB	Lysogeny broth
MDBK	Madin-Darby bovine kidney cells
MDP	methylenediphosphonate
MK455	{[3-(2-amino-6-oxo-1,6-dihydro-9H-purin-9-yl)-2-hydroxypropoxy]methyl}-phosphonic acid
MK520	{[3-(6-oxo-1,6-dihydro-9H-purin-9-yl)-2-hydroxypropoxy]methyl}-phosphonic acid
OD_{620}	optical density at 620 nm
PBS	phosphate buffered saline
PEEG	9-[2-(2-phosphonoethoxy)ethyl]guanine
PEEHx	9-[2-(2-phosphonoethoxy)ethyl]hypoxanthine
PEG 3350	poly(ethylene glycol) of average molecular weight 3350
PEG 400	poly(ethylene glycol) of average molecular weight 400
PEG 4000	poly(ethylene glycol) of average molecular weight 4000
*Pf*HGXPRT	*P. falciparum* hypoxanthine-guanine-xanthine phosphoribosyltransferase
PMEG	9-[2-(phosphonomethoxy)ethyl] guanine
PNP	purine nucleoside phosphorylase
*P*Rib-*PP*	5-phospho-α-D-ribosyl-1-pyrophosphate
PRTase	phosphoribosyltransferase
(*R,S*)-HPMPG	(*R,S*)-9-[3-hydroxy-2-(phosphonomethoxy)propyl]guanine
Tris	tris(hydroxymethyl)aminomethane
XGPRT	xanthine-guanine phosphoribosyltransferase
XMP	xanthosine 5'-monophosphate
ZMP	5-aminoimidazole-4-carboxamide-1-β-D-ribofuranosyl monophosphate

MASTER'S THESIS PART I: RESEARCH PROJECT REPORT

INTERACTION OF ACYCLIC NUCLEOSIDE PHOSPHONATES WITH THE TWO 6-OXOPURINE PHOSPHORIBOSYLTRANSFERASE PURINE SALVAGE ENZYMES FROM *E. coli*

1. INTRODUCTION

1.1. THE ROLE OF THE 6-OXOPURINE PHOSPHORIBOSYLTRANSFERASES

Purine nucleoside monophosphates, required for RNA and DNA synthesis, are produced via two metabolic pathways: *de novo* from small molecules or via salvage pathways from preformed nucleobases. 6-Oxopurine phosphoribosyltransferases (PRTases) are key enzymes in the purine salvage pathway (*Craig & Eakin, 2000*; *Musick, 1981*).

The 6-oxopurine PRTases catalyze the reaction of 6-oxopurine nucleobases (guanine, hypoxanthine or xanthine) with 5-phospho-α-D-ribosyl-1-pyrophosphate (*P*Rib-*PP*), leading to the generation of the corresponding nucleoside-5'-phosphates (GMP, IMP or XMP) and inorganic pyrophosphate (PP_i) (*Deo et al., 1985*). A divalent cation, such as magnesium, is essential for catalysis to occur. In the reaction, the ribose ring is the subject of an α-to-β anomeric conversion. The reaction is shown in Figure 1.1.

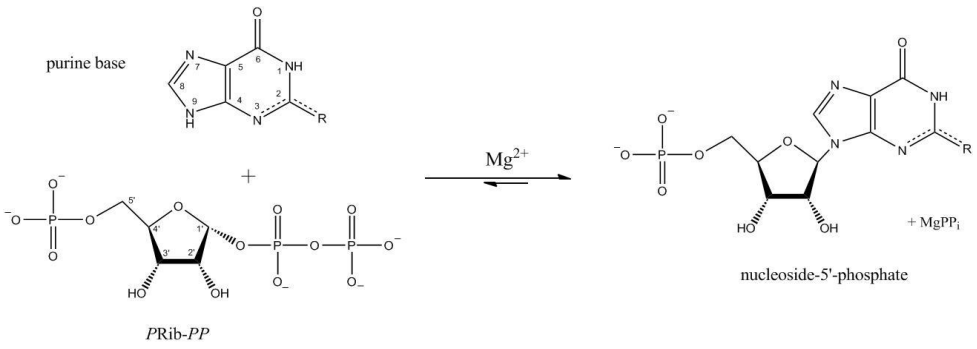

Figure 1.1. The reaction catalyzed by 6-oxopurine PRTases. The naturally occurring purine bases are guanine (R is $–NH_2$), hypoxanthine (R is –H) and xanthine (R is =O). The corresponding nucleoside-5'-phosphates are GMP (R is $–NH_2$), IMP (R is –H) and XMP (R is =O).

The 6-oxopurine PRTases are part of a group of enzymes, known as the phosphoribosyltransferases, that catalyze the formation of purine, pyrimidine and pyridine nucleotides and, in bacteria and lower eukaryotes, the formation of histidine and tryptophan (*Musick, 1981*). These enzymes have been studied for two reasons. Firstly, genetically inherited mutations in the DNA coding for human hypoxanthine-guanine phosphoribosyltransferase (HGPRT) result in serious diseases, known as Kelley-Seegmiller (*Seegmiller et al., 1967*) and Lesch-Nyhan syndromes (*Lesch & Nyhan, 1964*). Secondly, parasite protozoans are incapable of *de novo* purine synthesis and 6-oxopurine PRTases are essential for their growth and survival. Therefore, 6-oxopurine PRTases are considered to be promising drug targets in infections with parasitic protozoans such as *Plasmodium falciparum* (*Ting et al., 2005*) and *Leishmania donovani* (*Ullman & Carter, 1997*).

1.2. THE 6-OXOPURINE SALVAGE PATHWAY IN HUMANS

Disorders of purine metabolism in humans cause a variety of severe clinical symptoms. Inherited deficiency of HGPRT in humans is associated with hyperuricemia and a broad spectrum of neurological components (dystonia, ballismus, cognitive and attention deficit, self-destructive behavior) depending on the degree of enzymatic deficiency. The gene that codes for human HGPRT is located on the X chromosome (*Lesch & Nyhan, 1964*). The expressed gene is recessive, hence the disease generally affects males but there have been reported cases of affected females due to nonrandom inactivation of the normal X chromosome (*De Gregorio et al., 2000*).

Partial deficiency of human HGPRT is known as the Kelley-Seegmiller syndrome which is presented as a gout-urolithiasis syndrome (*Seegmiller et al., 1967*). Complete deficiency of human HGPRT activity results in the Lesch-Nyhan syndrome which also causes the overproduction of uric acid (*Lesch & Nyhan, 1964*). Other symptoms of this syndrome are choreoathetosis, mental retardation and self mutilation. Uric acid overproduction is caused by a pronounced activation of *de novo* purine synthesis and the degradation of hypoxanthine and guanine to uric acid as they are not reutilized in the absence of HGPRT. The mechanisms leading to the neurobehavioral abnormalities are unclear. It is hypothesized that *de novo* synthesis of purine nucleoside 5'-monophosphates in humans is not sufficient to provide all the necessary purine nucleoside 5'-monophosphates in the developing fetus (*Deutsch et al., 2005*). Another hypothesis is that the deficiency of HGPRT causes accumulation of a toxic metabolite, 5-aminoimidazole-4-carboxamide-1-β-D-ribofuranosyl monophosphate (ZMP), in the brain of Lesch-Nyhan disease patients (*López, 2008*). This metabolite is believed to cause (1) inhibition of mitochondrial oxidative phosphorylation and adenylosuccinate lyase activity, followed by cell death in the cerebellum and (2) prolonged activation of AMP-activated protein kinase causing reduction of dopamine synthesis and changes in neuronal morphology during development of the basal ganglia.

1.3. THE 6-OXOPURINE SALVAGE PATHWAY IN PROTOZOAN PARASITES

In contrast with other organisms that use both *de novo* synthesis and salvage pathways for the synthesis of purine nucleotides, all the parasitic protozoa and helminths studied so far lack the metabolic machinery to produce 6-oxopurine nucleoside 5'-monophosphates *de novo.* Therefore, they are entirely dependent on the transport of preformed nucleobases and nucleosides from the host cell. These metabolites cross the parasite membrane either actively (*Downie et al., 2006*) or passively (*Parker et al., 2000*). Because of the reliance of parasites on the purine salvage pathway for survival and replication, enzymes involved in this pathway were suggested as promising drug targets for the treatment of diseases caused by parasites more than 40 years ago (*Walsh & Sherman, 1968*).

Two species of protozoan parasites, *Plasmodium falciparum* and *Plasmodium vivax*, are the principal causative agents of malaria in humans, resulting in 1 to 2 million deaths yearly (*Breman, 2009*). The former species is generally found in Africa and is the most lethal parasite (*Lindsay & Martens, 1998*), while the later is more prevalent in Asia (*Mendis et al., 2001*). Both parasites rely entirely on the host for their source of 6-oxopurines. Figure 1.2 shows the interactions between the host and parasite purine pathways in erythrocytes that are infected with *P. falciparum*.

The completion of the *P. falciparum* genome sequencing project (*Gardner et al.,* 2002) and the sequencing of the genome of *P. vivax* (*Carlton, 2003*), confirmed that the 6-oxopurine salvage pathway was the only metabolic route for synthesis of the 6-oxopurine nucleoside monophosphates. The only 6-oxopurine salvage enzyme used by *P. falciparum* is hypoxanthine-guanine-xanthine PRTase (HGXPRT) and by *P. vivax* is HGPRT. These enzymes have therefore been confirmed as targets for chemotherapy because their catalytic activity is essential for the survival and replication of the parasites. Indeed, inhibitors of *Pf*HGXPRT arrest growth and division of the parasite (*Keough et al., 2009*). For example, 6-mercaptopurine and (*R,S*)-9-[3-hydroxy-2-(phosphonomethoxy)propyl]guanine ((*R,S*)-HPMPG), both exhibit IC_{50} values of 1 µM against *P. falciparum* cells grown in culture. 6-Mercaptopurine and 8-azaguanine have been found to arrest parasitemia in mice infected with the malarial strain of *P. berghei* with IC_{50} values of 47 and 32 µM, respectively (*Keough et al., 2006*). The mechanism of action of 6-mercaptopurine is different from inhibition of HGXPRT as 6-mercaptopurine is a substrate and the product of the catalytic reaction, 6-thio IMP, is toxic for the parasite after incorporation into DNA (*Elgemeie, 2003*).

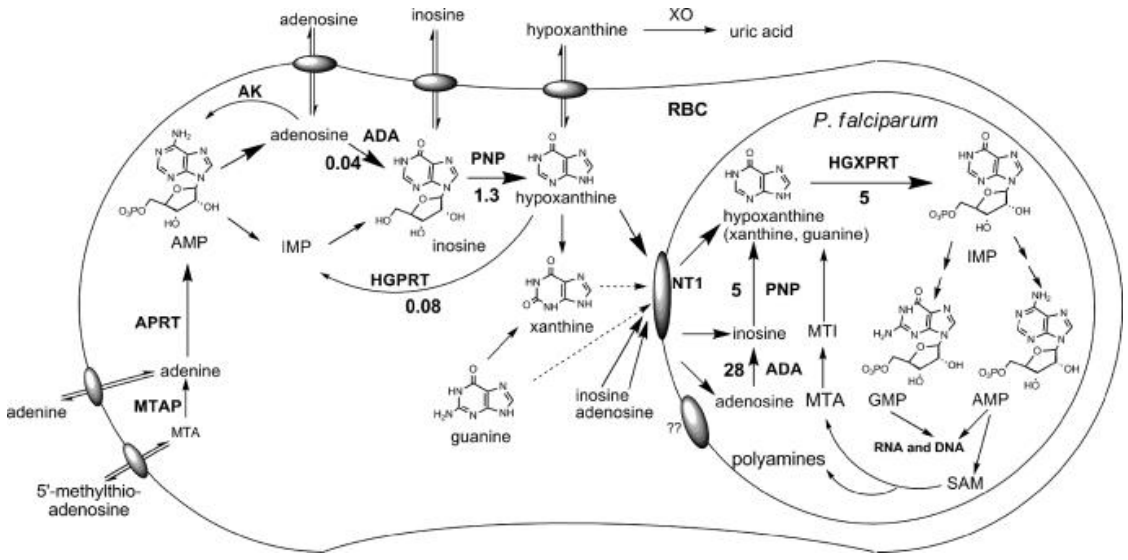

Figure 1.2. The interactions between the host and parasite purine pathways in erythrocytes that are infected with *P. falciparum.* Enzymes present in the erythrocyte cytosol are methylthioadenosine phosphorylase, adenine phosphoribosyltransferase (APRT), adenosine kinase, adenosine deaminase (ADA), purine nucleoside phosphorylase (PNP) and HGPRT. Enzymes present in *P. falciparum* are ADA, PNP and HGXPRT (*Madrid et al., 2008*).

1.4. THE 6-OXOPURINE PRTASES IN BACTERIA

Although bacteria are able to synthesize purine nucleotides *de novo*, 6-oxopurine PRTases are important in their metabolism. *Helicobacter pylori*, a Gram-negative, microaerophillic bacterium which causes gastric ulcers, uses xanthine-guanine phosphoribosyltransferase (XGPRT) for purine salvation. Disadvantages of the current therapies for *H. pylori* infections are the emergence of *H. pylori* strains resistant to antibiotics and the eradication of beneficial gastrointestinal flora through the use of broad-spectrum antibiotics (*Duckworth et al., 2006*). These problems suggest that the search for novel chemotherapeutic agents selective against this infection is strongly advisable. In this case, *H. pylori* XGPRT can be considered a potential target for chemotherapy because the enzyme appears to be essential for the survival of the bacterium (*Chalker et al., 2001*). The essentiality of XGPRT in *H. pylori* is surprising, considering that *H. pylori* is able to synthesize purine nucleotides *de novo* (*Mendz et al., 1997*). An unknown supplementary function, making the *H. pylori* enzyme necessary for survival, could be a possible explanation (*Chalker et al., 2001*).

In addition, it has been described that HGPRT is used as a component of the purine salvage pathway by *Mycobacterium tuberculosis*, the causative agent of most cases of tuberculosis (*Biazus et al., 2009*). HGPRT might be a favorable target for future drug development as there is a need of new agents with a different mechanism of action that can be used in combination therapy to control the expansion of *M. tuberculosis* strains that are resistant to current therapies.

Escherichia coli, a Gram-negative, facultatively anaerobic enteric bacterium, uses two 6-oxopurine PRTases in its 6-oxopurine salvage pathway, namely XGPRT and hypoxanthine phosphoribosyltransferase (HPRT) (*Gots & Benson, 1973; Neuhard & Nygaard, 1987*). Commensal *E. coli* strains are consistent inhabitants of the human intestinal tract. However, certain strains of *E. coli* are pathogenic and are responsible for three types of infections in humans: urinary tract infections, neonatal meningitis and intestinal diseases (gastroenteritis) (*Cooke, 1985*). One particular strain of this bacterium, O157:H7, is notorious for causing serious and even life-threatening complications like hemolytic uremic syndrome (*Griffin et al., 1988*). Furthermore, *E. coli* has the ability to quickly acquire drug resistance (*Paterson & Bonomo, 2005*; *National Institute Of Allergy And Infectious Diseases, 2001*) and a recent study indicates that treatment with known antibiotics does not improve the outcome of the disease, and may in fact significantly increase the chance of developing hemolytic uremic syndrome if infected with the virulent O157:H7 *E. coli* strain (*Wong et al., 2000*). For this reason, antibiotics using different mechanisms of action could help to suppress the increase of drug resistance and complications in pathogenic *E. coli* strains. Combination therapy, consisting of knock-out of *de novo* purine synthesis in *E. coli* (*Benson et al., 1970*) and inhibition of the two 6-oxopurine

salvage enzymes, could prove a viable option. The interactions between these two enzymes and their inhibitors will be investigated in this thesis.

1.5. THE 6-OXOPURINE SALVAGE PATHWAY IN *Escherichia coli* : COMPARISON OF THE PROPERTIES OF *E. coli* XGPRT AND HPRT

1.5.1. Comparison of kinetic constants for *E. coli* XGPRT and HPRT

E. coli XGPRT catalyses the conversion of guanine, xanthine and, to a lesser extent, hypoxanthine to GMP, XMP and IMP, respectively (*Deo et al., 1985*). A second *E. coli* 6-oxopurine salvage enzyme, hypoxanthine phosphoribosyltransferase (HPRT), primarily converts hypoxanthine to IMP. Both enzymes appear to be needed in the bacterium because they have a distinct substrate preference. Adenine phosphoribosyltransferase (APRT), which is a 6-aminopurine PRTase and converts adenine to adenosine monophosphate (AMP), is also present in *E. coli*. These three purine PRTases are components of the purine salvage pathway of *E. coli*. The crystal structure of *E. coli* XGPRT has been solved in both the absence and the presence of substrates and products (*Vos et al., 1997*; *Vos et al., 1998*) and *E. coli* HPRT has been solved in the absence of either substrates or products and in complex with IMP (*Guddat et al., 2002*). These results illustrate the structural changes which occur when the naturally occurring substrates or products bind.

In terms of catalytic efficiency, as indicated by k_{cat}/K_m values, *E. coli* XGPRT prefers guanine > xanthine > hypoxanthine (Table 1.1). In contrast, *E. coli* HPRT uses hypoxanthine as the preferred substrate, with the catalytic efficiency of hypoxanthine >> guanine >> xanthine. Therefore, both these enzymes are required to be present *in vivo* to efficiently convert the 6-oxopurine bases to their respective nucleoside monophosphates.

Table 1.1. *Comparison of kinetic constants for the naturally occurring substrates for wild type* E. coli *XGPRT and* E. coli *HPRT*[a,b]

	Specific activity (μmol min^{-1} mg^{-1})	$K_{m\ (app)}$ (μM)	k_{cat} (s^{-1})	k_{cat}/K_m (μM^{-1} s^{-1})
E. coli XGPRT (wild type)				
Hypoxanthine	23	90.8 ± 11.3	13.7 ± 1.1	0.2 ± 0.02
Guanine	95	4.3 ± 0.3	28.0 ± 0.4	6.5 ± 0.5
Xanthine	114	30.5 ± 2.6	37.5 ± 0.7	1.2 ± 0.1
*P*Rib-*PP*[c]	95	139 ± 16	28.0 ± 2	0.2 ± 0.25
E. coli HPRT				
Hypoxanthine	177	12.5 ± 2.4	59.0 ± 3.5	4.9 ± 1.2
Guanine	30	294 ± 20	10.2 ± 0.7	0.03 ± 0.005
Xanthine	0.02	25 ± 6.1	0.008 ± 0.0001	0.0003 ± 0.00003
*P*Rib-*PP*[d]	177	192 ± 7.0	50.0 ± 2	0.26 ± 0.04

[a] K_m values were measured in 0.1 M Tris-HCl, 0.012 M $MgCl_2$ at pH 7.40. [b] *Guddat et al., 2002*. [c] Guanine as the 6-oxopurine base substrate. [d] Hypoxanthine as the 6-oxopurine base substrate.

GMP and IMP, the products of the reaction catalyzed by 6-oxopurine PRTases, are competitive inhibitors of *E. coli* XGPRT and HPRT. For *E. coli* HPRT, the K_i value of IMP is more than 2-fold lower than that of GMP (Table 1.2), indicating that IMP binds more tightly to the enzyme than GMP, as would be expected from the enzyme's higher affinity for hypoxanthine (Table 1.1). The same conclusion can be drawn for *E. coli* XGPRT, as the 13-fold lower K_i value of GMP compared to IMP reflects the enzyme's higher affinity for guanine.

Table 1.2. *K_i values of nucleoside monophosphates for* E. coli *XGPRT and HPRT.*

	K_i (μM) GMP	K_i (μM) IMP
E. coli XGPRT[a]	4.5	60.3
E. coli HPRT[b]	526 ± 68	247 ± 55

[a] *Keough et al., unpublished results*. [b] *Guddat et al., 2002*.

1.5.2. Sequence and structure similarities and differences

The amino acid sequence identity between *E. coli* XGPRT and HPRT is 23%, which is low considering overlapping functions. In comparison, sequence identity between *P. falciparum* HGXPRT and *P. vivax* HGPRT is 77%. The monomeric subunits of the bacterial 6-oxopurine PRTases are smaller than those of the human, with the *E. coli* XGPRT monomer containing 152 amino acids, *E. coli* HPRT 182 amino acids, and human HGPRT 213 amino acids. Sequence identity between human HGPRT and *E. coli* XGPRT is 22 % and between human HGPRT and *E. coli* HPRT is 32 %, stating that *E. coli* HPRT is more closely related to the human enzyme. In solution, the active form of these three enzymes is tetrameric (*Vos et al., 1997*; *Guddat et al., 2002*; *Holden & Kelley, 1978*). Sequence alignment for *E. coli* XGPRT, *E. coli* HPRT and human HGPRT is shown in Figure 1.3.

The crystal structures of *E. coli* XGPRT and HPRT show a highly conserved core region, consisting of a four- or five-stranded parallel β-sheet surrounded by three or four α-helices. They also contain a highly flexible loop that has been proposed to close over the active site and shield the active site from solvent during catalysis (section 1.6) (*Scapin et al., 1994*). In addition to the core region and the flexible loop, the 6-oxopurine PRTases contain a hood region situated above the core and consisting of amino acid residues from the amino and carboxyl termini of the enzyme. In contrast to the core region, the structure of the hood is poorly conserved amongst the 6-oxopurine PRTases (*Guddat et al., 2002*).

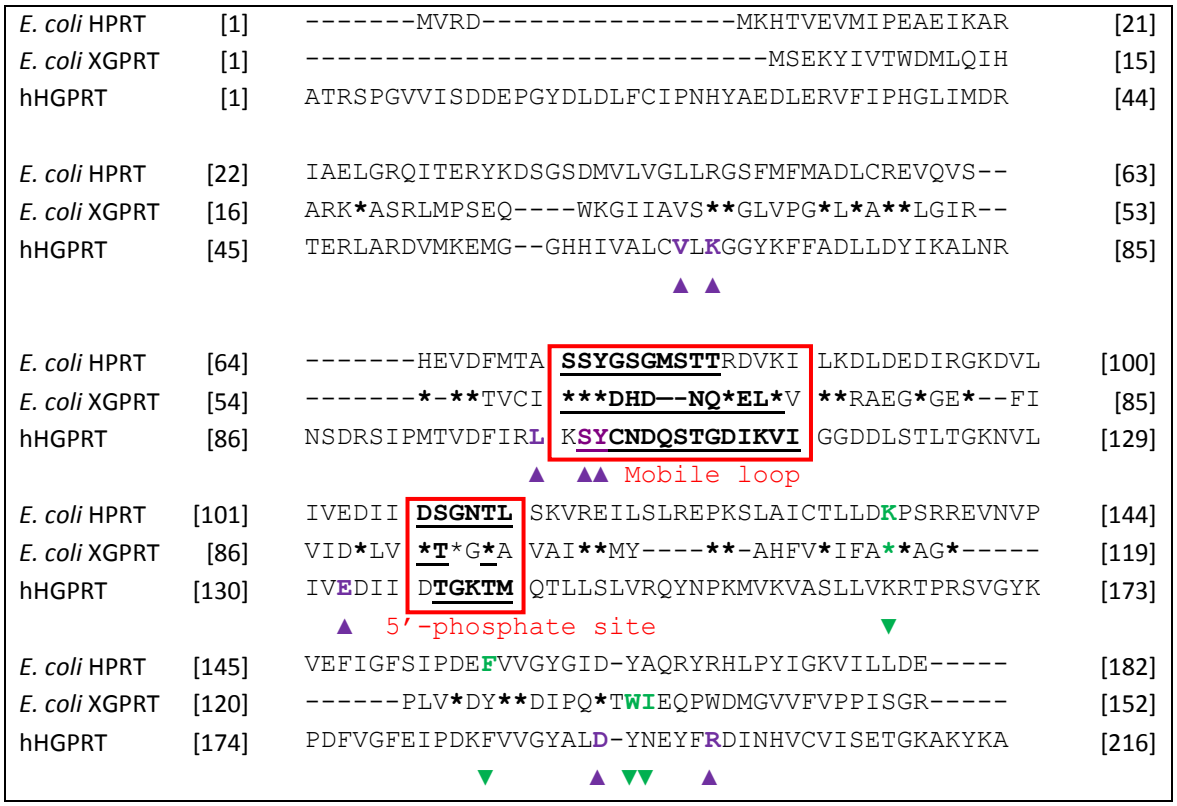

Figure 1.3. Alignment of the amino acid sequences of *E. coli* HPRT, *E. coli* XGPRT and human HGPRT. Identical residues between the *E. coli* enzymes are indicated with *. Green ▼ show the residues of *E. coli* XGPRT and *E. coli* HPRT that interact with the purine base of GMP and IMP, respectively. Purple ▲ denote the residues which hold pyrophosphate in place in human HGPRT (section 1.7). The 5'-phosphate binding residues and the residues that form a mobile loop (section 1.6) in the three enzymes are bold and underlined in a red box. The structures were aligned using the least squares fitting algorithm in the program O (*Jones et al., 1991*).

The nucleoside monophosphate products of the reaction, of which the inhibitors in this thesis are structural analogs, are competitive inhibitors of *E. coli* XGPRT and HPRT (section 1.5.1). In both enzymes, the 5'-phosphate group of the product (GMP and IMP) is anchored by an extensive network of hydrogen bonds (Figure 1.4). The amino acid residues involved in these interactions are Arg-69, Asp-92, Thr-93, Thr-96 in *E. coli* XGPRT and Asp-107, Ser-108, Gly-109, Asn-110, Thr-111 and Leu-112 in *E. coli* HPRT. The hydrogen bonds are formed with backbone nitrogens or side chains of these residues.

The purine base of the nucleoside 5'-monophosphate products interacts in two ways with these enzymes. Firstly, there are hydrophobic ring stacking interactions between the purine ring of GMP and Trp-134 in *E. coli* XGPRT and the purine ring of IMP and Phe-156 in *E. coli* HPRT. Secondly, there is a hydrogen bond between the 6-oxo group of the purine and a highly conserved lysine. This lysine residue, Lys-115 in *E. coli* XGPRT and Lys-135 in *E. coli* HPRT, plays a role in the specificity of both enzymes for 6-oxopurines versus adenine, a 6-aminopurine (*Eads et al., 1994*) as the interactions with the 6-oxo group are not possible when it is replaced by a 6-amino group.

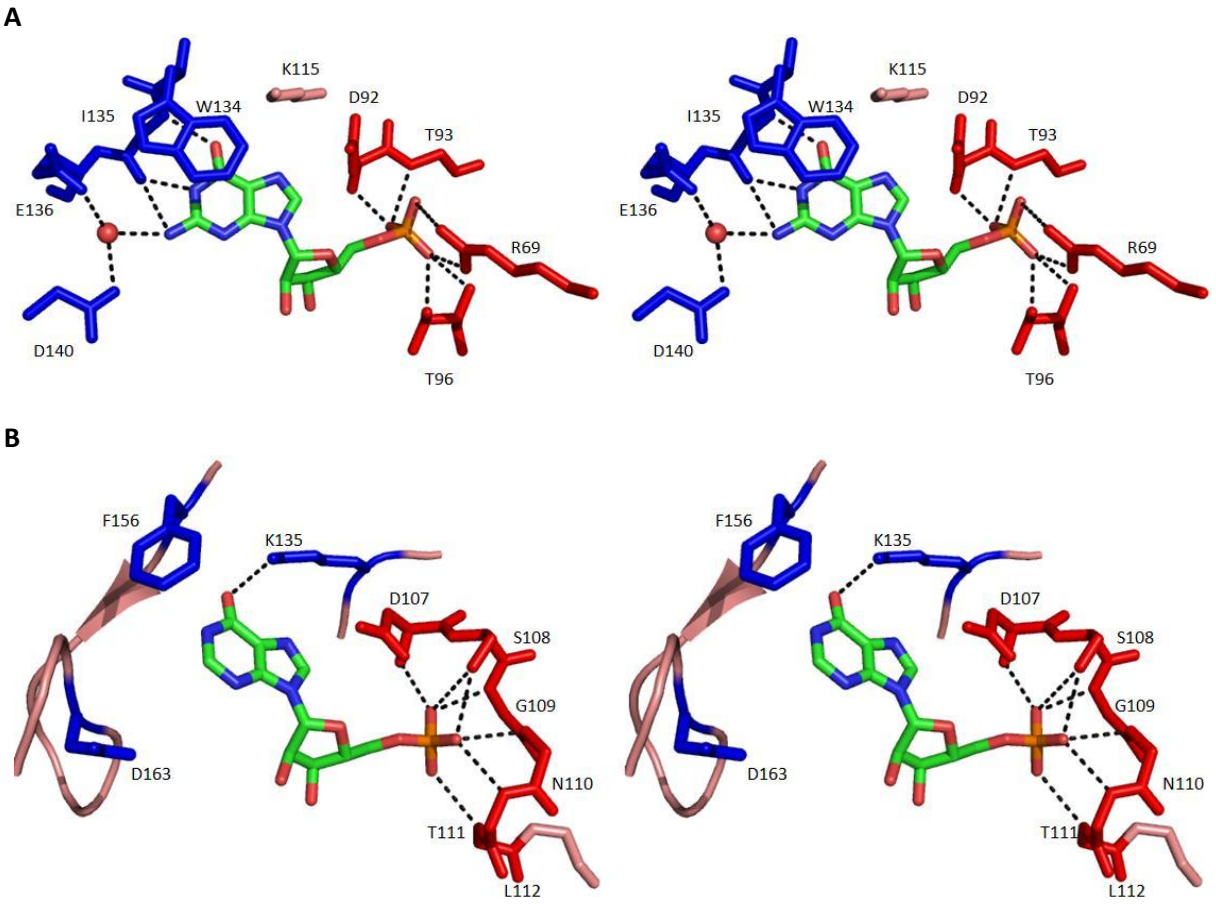

Figure 1.4. Stereo view comparing the active site residues in *E. coli* XGPRT and *E. coli* HPRT that interact with the nucleoside monophosphate products. Amino acid residues colored in red interact with the 5'-phosphate group, residues in blue interact with the purine base. **A** GMP bound to *E. coli* XGPRT. The red sphere is a water molecule. **B** IMP bound to *E. coli* HPRT. The side chain of Asp-163 does not form a hydrogen bond as there is no exocyclic N-atom in the hypoxanthine base of IMP. The guanine base in GMP has an NH_2-subsituent at position 2 that can form this hydrogen bond.

However, the distance between Lys-115 and the 6-oxo group of guanine in *E. coli* XGPRT is unexpectedly long (3.4 to 3.5 Å), whereas the distance between the backbone amide group of Ile-135 and the 6-oxo group is within hydrogen bonding distance (2.7 to 3.2 Å). Therefore, it has been proposed that specificity of *E. coli* XGPRT for 6-oxopurines versus 6-aminopurines is determined by the backbone amide group of Ile-135 rather than the side chain of Lys-115 (*Vos et al., 1998*).

The ribose rings of GMP and IMP are not themselves involved in direct interactions with residues of *E. coli* XGPRT and HPRT. There is no magnesium ion present in the structures with GMP or IMP bound, though a magnesium ion is seen in the free crystal structures. Magnesium ions have not been found in any of the solved structures with nucleoside 5'-monophosphates as the magnesium ion leaves the active site complexed to PP_i after formation of the product (*Vos et al., 1998*).

Discrimination of the *E. coli* enzymes between the 6-oxopurine base substrates is based on the difference in the group in the 2-position in all three 6-oxopurine base substrates (Figure 1.1). It is

hypothesized that *E. coli* XGRPT discriminates between the three naturally occurring 6-oxopurine bases through interaction with the carbonyl oxygen of the backbone of Ile-135 (Figure 1.4). This carbonyl oxygen forms a hydrogen bond with the 2-amino group of guanine, but not with the 2-oxo group of xanthine. The 2-exocyclic groups of both xanthine and guanine are also stabilized by a water-mediated interaction with the side chains of Glu-136 and Asp-140. The hydrogen atom of hypoxanthine in the 2-position cannot participate in interactions with either a water molecule or the backbone carbonyl oxygen of Ile-135 (*Vos et al., 1998*). For *E. coli* HPRT, it is hypothesized that the carbonyl oxygen of Asp-163 is responsible for discrimination between these three 6-oxopurine bases. The carbonyl oxygen forms a hydrogen bond with the N-atom at position 2 in the guanine base of GMP, forcing it to adapt a different position in the active site and allowing the catalytically important side chain of Asp-107 to rotate away from the purine base. This is not the case in IMP, as hypoxanthine does not have an N-atom at position 2 and could explain the fivefold higher k_{cat} for hypoxanthine compared to guanine. In addition, the carbonyl oxygen of Asp-163 would repel the 2-exocyclic oxygen in xanthine, forcing this purine base too to adopt a different and less desirable position in the active site, compared to hypoxanthine (*Guddat et al., 2002*).

1.6. THE ROLE OF THE MOBILE LOOP

Residues 61 to 72 of *E. coli* XGPRT and residues 73 to 82 of *E. coli* HPRT form a highly flexible loop. It has been proposed that this loop closes over the active site during catalysis to shield the transition state in the active site from solvent (*Scapin et al., 1994*). The investigation of the role of the flexible loop of *E. coli* XGPRT in binding of acyclic nucleoside phosphonate inhibitors (section 1.7) forms part of this thesis.

Proteolytic cleavage of residues 66 to 76 in *E. coli* XGPRT resulted in almost complete loss of activity (*Vos et al., 1997*). It was suggested that the loss in catalytic activity may be due to an inability to shield the active site from solvent or the removal of any or all of the positively charged residues Arg-69, Lys-72, Lys-75 and Arg-76 (*Vos et al., 1997*). The role of the mobile loop in catalysis or binding to substrates and inhibitors has been investigated by the preparation of a mutant recombinant *E. coli* XGPRT (called loop-out). In this mutant enzyme, residues 61 to 72 were replaced by a single alanine.

Removal of the flexible loop in *E. coli* XGPRT did not greatly affect the binding of the purine bases or *P*Rib-*PP* (Table 1.3). This is expected as, for the substrates to enter the active site, the loop is open. However, removal of the mobile loop had a marked effect on the k_{cat}, decreasing it 200-fold. The removal of the loop also increases the K_i for the nucleoside monophosphate products, as the K_i value for loop-out XGPRT is 120 μM for GMP. Thus, the mobile loop plays a role in catalysis and in the binding of the reaction products.

Table 1.3. *Kinetic constants for the naturally occurring substrates for* E. coli *loop-out XGPRT*[a]

	$K_{m\ (app)}$ (μM)	k_{cat} (s^{-1})	k_{cat}/K_m ($\mu M^{-1}\ s^{-1}$)
E. coli loop-out XGPRT [b]			
Guanine	1.72 (4.3)	0.136 (28)	0.079 (6.51)
Xanthine	30.3 (31)	0.113 (37.5)	0.004 (1.21)
*P*Rib-*PP*[c]	61 ± 6 (64.3)	0.140 (28)	0.002 (0.44)

[a] K_m values were measured in 0.1 M Tris-HCl, 0.012 M $MgCl_2$ at pH 7.40. [b] *Keough et al., unpublished results*. Kinetic constants of wild type *E. coli* XGPRT are shown in brackets. [c] Guanine as the 6-oxopurine base substrate.

1.7. HUMAN HGPRT

The structure of human HGPRT has been solved in the absence and presence of a series of ligands and inhibitors: GMP (*Eads et al., 1994*), 7-hydroxy [4,3-d] pyrazolo pyrimidine (HPP) in the presence of Mg^{2+}.*P*Rib-*PP* (*Balendiran et al., 1999*), acyclic nucleoside phosphonates (*Keough et al., 2009*) and immucillinGP.Mg^{2+}.PP_i (*Shi et al., 1999*). ImmucillinGP (ImmGP) is a transition state analog of the reaction. GMP, with a K_i of 5.8 ± 0.2 μM, binds more weakly to the enzyme (*Giacomello & Salerno, 1978*) than some acyclic nucleoside phosphonates (ANP) (K_i = 1.0 μM; 3.6 μM; 5.9 μM for the ANPs 9-[2-(2-phosphonoethoxy)ethyl]guanine (PEEG), 9-[2-(2-phosphonoethoxy)ethyl]hypoxanthine (PEEHx) and (*R,S*)-HPMPG, respectively) (*Keough et al., 2009*). The transition state analog immucillinGP, bound together with Mg^{2+}.PP_i, is the inhibitor with the tightest binding to the enzyme known so far as it inhibits the reaction with equilibrium binding constants that are > 1000-fold higher than those for the nucleoside 5'-monophosphate substrates (*Li et al., 1999*). ImmGP binds more tightly in the presence of Mg^{2+}.PP_i.

In the crystal structure of human HGPRT in the presence of GMP, the mobile loop is not ordered and not visible as the reaction product is preparing to leave the active site (*Eads et al., 1994*). However, when the ANP inhibitor 9-[2-(2-phosphonoethoxy)ethyl]guanine (PEEG) is bound, the loop is ordered and partly covers the active site (*Keough et al., 2009*). In the structure of human HGPRT bound to ImmGP.Mg^{2+}.PP_i, the mobile loop is ordered and completely closes over the active site (*Shi et al., 1999*). It is assumed that the tight binding of ImmGP is due to binding of PP_i in a pyrophosphate binding pocket. These three positions of the loop are shown in Figure 1.5.

The pyrophosphate binding pocket in human HGPRT consists of the amino acid residues Val-66, Lys-68, Leu-101, Glu-133, Asp-193, Arg-199 (*Shi et al., 1999*). These residues form an extensive network of hydrogen bonds with the oxygen atoms of PP_i either directly or mediated through water molecules and/or one of the two Mg^{2+} ions (*Shi et al., 1999*). Residues of the flexible loop (Ser-103

and Tyr-104) also interact directly with oxygen atoms of PP_i. The pyrophosphate binding pocket is visualised in Figure 1.6.

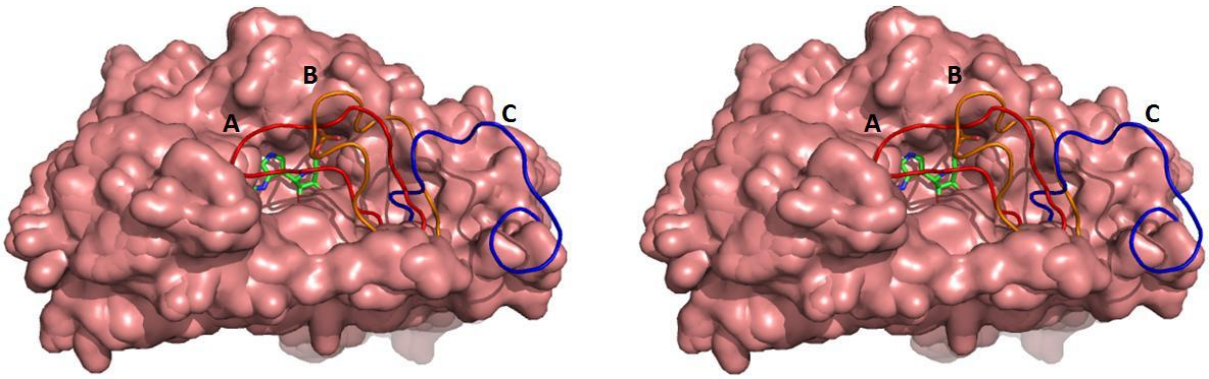

Figure 1.5. Stereo view of the position of the mobile loop in human HGPRT with bound inhibitors. The position of the mobile loop is shown in the structure of human HGPRT bound to GMP, PEEG and ImmGP.PP_i.Mg^{2+}. The only compound that is shown as a stick model in the active site, is ImmGP. **A** The loop completely covers the active site when ImmGP.PP_i.Mg^{2+} is bound. **B** The loop is ordered and partly covers the active site as PEEG, an acyclic nucleoside phosphonate, is bound. **C** The flexible loop is in an open conformation when GMP is bound as the product and is preparing to leave the active site. Due to poor electron density for the loop-forming residues, a hypothetical loop has been visualised in the position it is assumed to occupy.

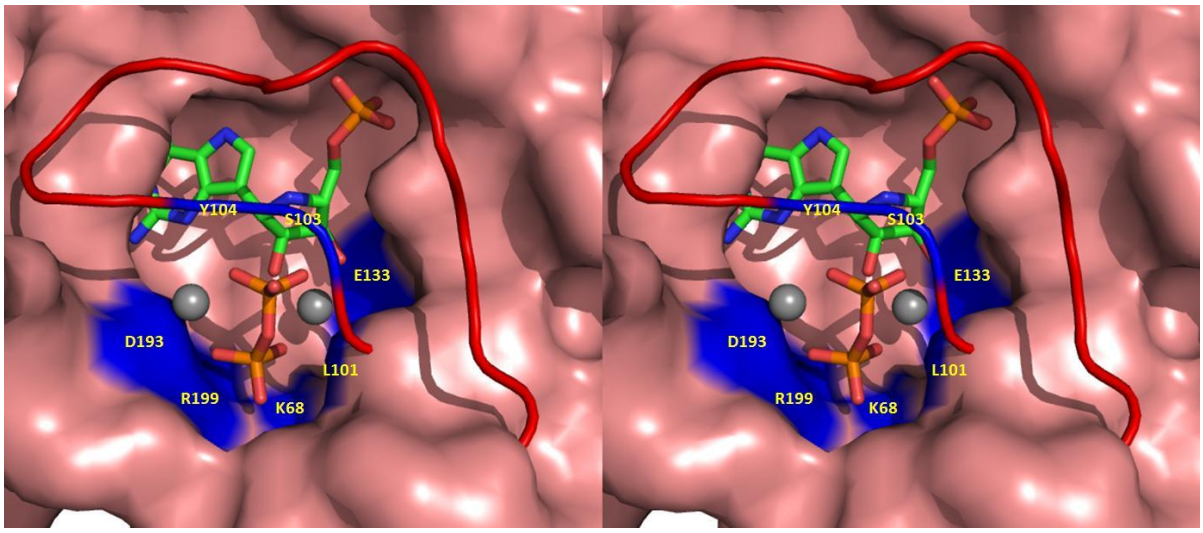

Figure 1.6. Stereo view of the PP_i binding pocket in human HGPRT. ImmGP is bound in the active site (and shown as a stick model), together with PP_i and two Mg^{2+} ions (shown as grey spheres). The mobile loop is colored in red, the residues that interacts with PP_i are shown in blue.

PP_i cannot bind in the pyrophosphate binding pocket in the presence of the purine base and *P*Rib-*PP* as the pyrophosphoryl group of *P*Rib-*PP* occupies the pyrophosphate binding pocket and thereby inhibits binding of PP_i (*Shi et al., 1999*). On the other hand, ImmGP can only bind human HGPRT when PP_i binds in the pyrophosphate binding pocket. It is hypothesized that only in the presence of PP_i, the loop can close completely over the active site and interactions of ImmGP and Mg^{2+}.PP_i with the loop stabilize this closed state so the enzyme cannot bind substrate (*Shi et al., 1999*).

Of the eight residues that interact with PP_i in human HGPRT, five residues are identical and three residues are conserved in *E. coli* HPRT. In *E. coli* XGPRT, four identical and three conserved residues

can be seen. These data indicate a similar pocket in the *E. coli* enzymes, where binding of PP_i could also help to close the loop in the presence of the ANPs.

1.8. ACYCLIC NUCLEOSIDE PHOSPHONATES

The acyclic nucleoside phosphonates (ANPs) studied in this thesis are structural analogs of the reaction products catalyzed by PRTases and are 2-(phosphonoalkoxy)alkyl derivatives of purine bases. ANPs with a pyrimidine or a 6-aminopurine base attached have been the subject of intensive study as they have been developed as antiviral therapeutics (*De Clercq et al., 1986*; *De Clercq et al., 1987*). The ANPs investigated in this thesis contain a 6-oxopurine base instead of a pyrimidine or 6-aminopurine base and this group of ANPs are known inhibitors of human HGPRT (*Keough et al., 2009*), *P. falciparum* HGXPRT (*Keough et al., 2009*), *P. vivax* HGPRT (*Keough et al., 2010*), *E. coli* XGPRT (*Keough et al., unpublished*) and *E. coli* HPRT (*Keough et al., unpublished*).

In the structure of the ANPs, there are three distinct parts that influence binding to the 6-oxopurine PRTases (Figure 1.7). These consist of a purine base (group A) and a phosphonate group (group B) that are linked by a series of atoms (group C). The combined effect of these three groups on the affinity of the compounds for the enzymes can be additive, synergistic or they can negate each other (*Keough et al., 2009*).

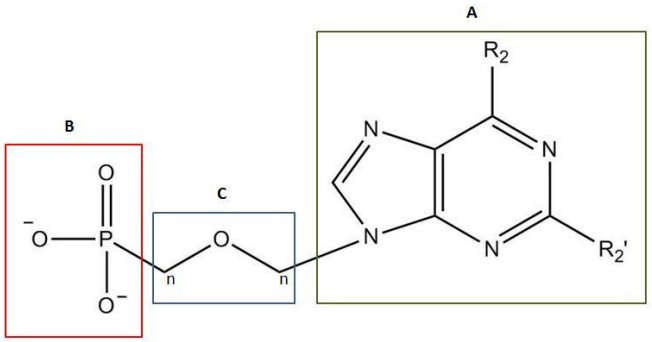

Figure 1.7. General structure of the acyclic nucleoside phosphonates. The ANPs consist of a purine or pyrimidine base (group A) which is connected by a alkoxyalkyl group (group C) to a phosphonate moiety (group B).

In the linker and phosphonate parts of the ANPs, three differences can be noticed, compared to the product nucleoside 5'-monophosphate of the reaction. Firstly, the position of the oxygen atom is altered compared with the position it would normally occupy in the ribose ring in one of the nucleoside 5'-monophosphate products. Secondly, in the phosphonate part of the structure, there is no longer an ester oxygen atom available for dephosphorylation or hydrolysis because it is replaced by a carbon atom. This replacement makes the ANPs resistant to cleavage by phosphatase enzymes. Thirdly, susceptibility of the ANPs to chemical or enzymatic degradation is even more decreased due to the absence of a labile glycosidic bond. Another advantage of the ANPs is the high level of

flexibility of the linker, which allows these compounds to adopt a conformation suitable for interaction with the active site of the target enzyme.

The ANPs in general have favorable pharmacokinetic properties and have low cytotoxicity in mammalian cells. The ANPs investigated in this thesis were synthesized as inhibitors of 6-oxopurine PRTases in the context of antimalarial drug development. *In vitro* inhibition studies show that three ANPs – different from the ANPs investigated in this thesis – have an IC_{50} value for *P. falciparum* grown in cell culture of 1 µM, 14 µM and 45 µM, while the cytotoxic concentration for the first compound was 489 µM (*Keough et al., 2009*). A level of selectivity of these compounds for the parasite enzyme over the human enzyme has been observed. This is favorable as inhibition of human HGPRT could have serious side effects (section 1.2). However, reduction of human HGPRT to 3% of its normal activity in patients with congenital partial deficiency of HPRT has shown to have limited effects on normal life (*Keough et al., 2009*). Uric acid overproduction, which is the only drawback of the enzyme's inhibition, can be managed by allopurinol treatment. Therefore, it is unlikely that a drug which partially inhibits human HGPRT will have major repercussions.

2. AIMS

The 6-oxopurine phosphoribosyltransferases (PRTases) synthesize the 6-oxopurine nucleoside monophosphates essential for RNA and DNA production and they have been suggested as promising drug targets. Acyclic nucleoside phosphonates (ANPs) are structural analogs of the nucleoside monophosphate reaction products catalyzed by the 6-oxopurine PRTases (GMP, IMP and XMP). The ANPs in general have favorable pharmacokinetic properties and have low cytotoxicity in mammalian cells.

The aims of this thesis are to investigate the potential inhibition of the two *E. coli* 6-oxopurine PRTases (*E. coli* XGPRT and HPRT) by three ANPs and to investigate whether the removal of the mobile loop effects the binding of these ANPs.

AIM 1. To determine the K_i values for the ANPs for wild type *E. coli* XGPRT, mutant loop-out *E.* coli XGPRT and wild type *E. coli* HPRT. The three phosphonate compounds studied here are: DR3876, which contains a guanine base and a cyclic phosphonate part; MK520, which contains a hypoxanthine and an acyclic phosphonate part; and MK455, which contains a guanine and the same acyclic phosphonate part as MK520. The two *E. coli* enzymes exhibit different base specificity tor the three naturally-occurring purine bases, hypoxanthine, guanine and xanthine and, thus, the contribution of the purine base in the affinity of the ANPs can be ascertained. In addition, the hypothesis is that the closure of this loop, thereby covering the active site, is critical to achieve low K_i values for the ANPs.

AIM 2. To crystallize wild type *E. coli* XGPRT in complex with one of the ANPs.

AIM 3. To use proton NMR in preliminary experiments to investigate if any changes can be seen in the spectrum of *E. coli* XGPRT when an ANP binds.

3. MATERIALS AND METHODS

3.1. CHEMICALS AND REAGENTS

The 6-oxopurine bases (guanine, xanthine and hypoxanthine), GMP, PP_i, foscarnet, methylenediphosphonate (MDP), dithiothreitol (DTT), phenylmethylsulfonyl fluoride (PMSF), lysozyme, kanamycine and *P*Rib-*PP* were purchased from Sigma-Aldrich (St. Louis, United States). The purity of the 6-oxopurine bases, GMP, PP_i, foscarnet, MDP, DTT and PMSF was $\geq$ 99%. Ampicillin was purchased from Amresco (Ohio, United States). Tryptone was achieved by Becton, Dickinson and Company (Sparks, United States). Granulated yeast extract was obtained from Merck (Sydney, Australia). NMR Sample Tubes (5mm thin wall, 7" length, 500 MHz) were purchased from Wilmad Labglass (New Jersey, United States). Water was purified by a Millipore Milli-Q system (North Ryde, Australia).

Stock solutions of the 6-oxopurine bases were prepared in water with the addition of a small amount of 2 M NaOH to dissolve them. A stock solution of *P*Rib-*PP* was prepared in water and the purity was determined enzymatically by a method developed by the University of Queensland. This method involves 1 ml of assay buffer (0.1 M Tris-HCl, 0.012 M $MgCl_2$, pH 7.4), 60 µM of guanine, 1 µl of wild type *E. coli* XGPRT (5 mg/ml stock solution) and 10 µl of 1:10 *P*Rib-*PP* (10 mg/ml stock solution) in a total cuvette volume of 1041 µl. As the concentration of guanine in the assay is considerably higher than the concentration of *P*Rib-*PP*, all the *P*Rib-*PP* will be used for the conversion of guanine to GMP. Thus, the concentration of *P*Rib-*PP* and thereby its purity can be calculated from the change in absorbance when the reaction is complete. The precise concentration of *P*Rib-*PP* is determined as the compound is not supplied as 100% pure. The conversion of guanine to GMP is measured at 257.5 nm with an extinction coefficient ($\Delta\varepsilon$) of 5816.5 M^{-1} cm^{-1}.The equations that were used for this calculation are $A_{100\%} = \varepsilon.c.l$ and P (purity) = 100 (A_{obs} / $A_{100\%}$). Purity of the prepared *P*Rib-*PP* solutions varied from 64.2 % to 69.3 %, resulting in stock concentrations of 12.7 mM to 14.0 mM.

3.2. GENERAL METHODS

All assays and spectrophotometric measurements were performed using a Shimadzu UV-2501 spectrophotometer (Tokyo, Japan) fitted with a temperature controlled cell compartment, coupled to Shimadzu UV Probe software for data collection. All assays were performed at 25°C in 1 ml quartz cuvettes. A 901-PH pH-mV-Temperature meter from TPS (Brisbane, Australia) fitted with an IJ44C electrode from Ionode (Tennyson, Australia), was used for all pH measurements. The pH was calibrated using pH 7 and pH 10 BDH ® Reference Standard buffers. Enzyme concentration was

performed using a Millipore Amicon ® Ultra-4 centrifugal filter tube fitted with a Millipore Ultracel ® regenerated cellulose low binding membrane.

For volumes up to 50 ml, centrifugations were performed on a Beckman GS-6R centrifuge equipped with a GH-3.8 rotor, at 4°C and 3 000 g. For volumes ranging from 50-1000 ml, an Avanti J-26 centrifuge equipped with a JLA-9.1000 rotor was used, at 4°C and 3 500 g. Centrifugation of eppendorf tubes was performed on a Hermle Z 233 MK-2 microcentrifuge equipped with a C0230-2A rotor, at 4°C and 12 000 g.

3.3. SYNTHESIS OF ANPs AND ENZYME PREPARATION

Acyclic nucleoside phosphonates were synthesized in Professor Antonín Holý's laboratory (Prague) by Dominik Rejman and Marcela Kreěmerová. The purity of all the ANPs was > 95%. Recombinant wild type and loop-out *E. coli* XGPRT were expressed in *Escherichia coli* SΦ606 [*are, Δpro-gpt-lac, thi, hpt, F-*] cells and purified in Professor Luke Guddat's laboratory. Aliquots of 200 µl of purified enzyme in 0.05 M Tris-HCl, 0.01 M $MgCl_2$, 1 mM DTT, pH 7.4 were stored at -70°C. They are stable under these conditions for at least one year. Recombinant *E. coli* HPRT was also expressed, purified and stored in aliquots of 200 µl of enzyme in the same conditions as described above.

As part of this project, wild type *E. coli* XGPRT was expressed in *E. coli* SΦ606 [*ara, Δpro-gpt-lac, thi, hpt, F-*] cells as described by *Free et al. (1990)* to gain experience in enzyme expression. This method uses the T7 RNA Polymerase/Promotor system (*Tabor & Richardson, 1985*). This technique has a number of benefits compared to approaches that rely on *E. coli* RNA polymerase. First, T7 RNA polymerase is a very active enzyme: it synthesizes RNA at a rate several times that of *E. coli* RNA polymerase and it terminates transcription less frequently. Second, T7 RNA polymerase is highly selective for initiation at its own promoter sequences and it does not initiate transcription from any sequences on *E. coli* DNA. In the basic protocol, two plasmids are maintained within the same *E. coli* cell. One (the expression vector; pT7-7) contains the T7 RNA polymerase promoter (p_{T7}) upstream of the gene to be expressed. The second plasmid (pGP1-2) contains the T7 RNA polymerase gene under the control of a heat-inducible *E. coli* promoter (p_L). Upon heat induction, the T7 RNA polymerase is produced and initiates transcription on the expression vector, resulting in turn in the expression of the gene under the control of p_{T7}, which in this case is the *E. coli* XGPRT gene.

The *E. coli* cells, containing the two plasmids described above, were grown in an enriched SΦ606 media (20 g/l tryptone, 10 g/l yeast extract, 5 g/l NaCl, 2.5 g/l glycerol, 1.5 g/l KH_2PO4, 6.8 g/l K_2HPO4, 100 µg/ml ampicillin and 50 µg/ml kanamycin) at pH 7.3. The initial culture was 2×5ml of media with the cell line from previous glycerol stocks. Next, 2×100 ml overnight cultures were

transferred to inoculate 2×1 L of fresh media. The cells were grown in a Bio-Line incubator shaker at 30˚C and 185 RPM for 4.5 hours until an optical density of 1.6 at 600 nm was reached.

Expression was induced by heat shock at 42˚C for 45 minutes in a water-bath. This caused derepression of the p_L promoter controlling expression of T7 RNA polymerase from pGP1-2. The T7 RNA polymerase then binds to the T7 RNA promoter on the recombinant plasmid (pT7-7) enabling transcription of wild type *E. coli* XGPRT cDNA (*Tabor & Richardson, 1985*). Following heat shock, the culture was returned to the 30˚C incubator at 185 RPM to allow enzyme expression. The cells were collected by centrifugation at 3500 g and 4˚C for 20 minutes, then the cells were resuspended in 0.05 M Tris-HCl containing 1 mM DTT, 1 mM PMSF, 200 µM *P*Rib-*PP*, 0.01 M $MgCl_2$, pH 7.4 at 1/20 of the original volume and aliquots of 1 ml of cell paste were stored at -70˚C.

Lysozyme was added to 1 ml of thawed cell paste in an eppendorf tube (final concentration 1 mg/ml). The cell paste was incubated on ice for 60 minutes and freeze/thawed three times in liquid nitrogen before centrifugation at 12 000 g for 2 minutes at 4˚C. The supernatant was assayed in order to determine enzyme activity and quantity. This assay involved: 1 ml of assay buffer, 50 µM of guanine, 600 µM of *P*Rib-*PP* and 1 µl of supernatant in a total cuvette volume of 1 081 µl. The conversion of guanine to GMP was measured at 257.5 nm with $\Delta\varepsilon = 5816.5\ M^{-1}\ cm^{-1}$ and the enzyme concentration was calculated using a specific activity of 100 000 µmol min^{-1} mg^{-1} (*Vos et al., 1998*). Enzyme activity and enzyme concentration were determined using the equations:

(a) enzyme activity = (mAbs/min) $(V_{cuvette\ total})\ 10^6\ (\Delta\varepsilon)^{-1}\ (V_{enzyme\ solution})^{-1}$ (dilution factor)

(b) enzyme concentration = (enzyme activity) $(\text{specific activity})^{-1}$

Two liters of the loop-out recombinant *E. coli* XGPRT were also expressed and the cell paste stored at -70°C.

3.4. CORRELATION BETWEEN $[E]_0$ and V_{max}

The assays for determination of the correlation between $[E]_0$ and V_{max} comprised 1 ml of assay buffer, 50 µM guanine base and 600 µM *P*Rib-*PP* in a total cuvette volume of 1180 µl. An aliquot of wild type or loop-out *E. coli* XGPRT was diluted to several dilutions in assay buffer with 1mM DTT and added to the cuvette. During the assay, the concentration of wild type enzyme ranged from 0.6 to 3.7 nM in terms of subunits (with 4 subunits per enzyme molecule). The concentration of loop-out enzyme ranged from 140.8 to 706.8 nM in terms of subunits. The conversion of guanine to GMP was measured at 257.5 nm with $\Delta\varepsilon = 5816.5\ M^{-1}\ cm^{-1}$. Microsoft Excel was used for plotting of the data and calculation of the R^2-value.

3.5. DETERMINATION OF ENZYME CONCENTRATION

The enzyme concentration of purified wild type *E. coli* XGPRT was determined as described in section 3.3. In the assay, 1 ml of assay buffer, 55 µM guanine and 655 µM *P*Rib-*PP* in a total cuvette volume of 1 081 µl was used. The amount of enzyme in the cuvette was 1 µl of a 1:100 dilution of purified wild type *E. coli* XGPRT stock. The equations that were used for this calculation are equations (a) and (b) (section 3.3).

3.6. DETERMINATION OF KINETIC CONSTANTS

A continuous spectrophotometric assay was used to measure the kinetic constants for the purine bases, guanine, xanthine, and hypoxanthine, by following their conversion to GMP at 257.5 nm ($\Delta\varepsilon$ = 5816.5 M^{-1} cm^{-1}), XMP at 255 nm ($\Delta\varepsilon$ = 4685 M^{-1} cm^{-1}), and IMP at 245 nm ($\Delta\varepsilon$ = 2439 M^{-1} cm^{-1}), respectively (*Keough et al., 1987*). The assays were performed in quartz cuvettes with 1 ml of assay buffer and enzyme concentrations were 3.25 nM, 440 nM and 4.11 nM for *E. coli* wild type XGPRT, *E. coli* loop-out XGPRT and *E. coli* HPRT, respectively. Assays for the determination of K_m values for *P*Rib-*PP*, were performed with a guanine concentration fixed at 50 µM and a *P*Rib-*PP* concentration range of 14-430 µM depending on the K_m value. This concentration range has to include concentrations higher and lower than the K_m value to assure accurate determination of the K_m value. Assays for the determination of the K_m values for guanine were performed with a *P*Rib-*PP* concentration fixed at 570 µM and a guanine concentration range of 0.9-13.4 µM depending on the K_m value. The assays for the determination of the K_m value for xanthine and hypoxanthine were performed with a *P*Rib-*PP* concentration fixed at 455 µM and 460 µM, respectively, and a xanthine and hypoxanthine concentration range of 23-68 µM and 35-89 µM, respectively. K_m and V_{max} values for the naturally occurring substrates of the three *E. coli* enzymes were determined using Hanes-Woolf plots (*Hanes, 1932*). A Hanes–Woolf plot is a graphical representation of enzyme kinetics in which the ratio of the initial substrate concentration [S] to the reaction velocity v is plotted against $[S]_0$. Assay results will yield a straight line of slope $1/V_{max}$, a y-intercept of K_m/V_{max} and an x-intercept of $-K_m$. Data are represented as the mean ± SD.

3.7. DETERMINATION OF K_i VALUES

The K_i values were determined using a spectrophotometric assay with the same extinctions coefficients, wavelengths and enzyme concentrations as previously mentioned (section 3.6).

The concentration of GMP was 17 µM for the K_i value determination for wild type *E. coli* XGPRT and 90 µM for loop-out *E. coli* XGPRT. The concentration of guanine was fixed at 50 µM and the *P*Rib-*PP* concentration ranged from 41-412 µM, depending on the value of $K_{m(app)}$.

For determination of the K_i values for the ANPs, the concentration of *P*Rib-*PP* ranged from 26-895 µM, depending on the value of $K_{m(app)}$ at a fixed concentration of inhibitor. The concentration of guanine – for both *E. coli* XGPRT enzymes – or hypoxanthine – for *E. coli* HPRT – was fixed at 50 µM. The concentration of inhibitor ranged from 0.88 µM (for the best inhibitor) to 32 µM (for the weakest inhibitor). K_i values were determined by Hanes-Woolf plots and calculated using Prism (GraphPad Software, Inc., La Jolla, United States). Data are represented as the mean ± SD. In certain cases, K_i values were calculated using the equations $K_{m\ (app)} = K_m\ (1+ ([I]/K_i)\ )$ and $v_0 = (V_{max}\ [S]_0) / (K_m + [S]_0)$. These equations will be referred to in the results section as equation (1) and equation (2), respectively. In competitive inhibition, the maximum velocity (V_{max}) of the reaction is unchanged, while the K_m value is increased.

3.8. EFFECT OF PYROPHOSPHATE

Prior to the investigation of the effect of PP_i on the ANP inhibitors, it was tested whether PP_i itself would act as an inhibitor of the *E. coli* enzymes. Wild type *E. coli* XGPRT and *E. coli* HPRT were not inhibited by 34 µM of PP_i in the conditions that will be used to test the effect of PP_i on inhibition by the ANPs. In the assays with ANP inhibitors, the PP_i concentration ranged from 32-34 µM and was always higher than the concentration of the ANP inhibitor.

In the next step, the effect of foscarnet and methylenediphosphonate (MDP) on the inhibition of wild type *E. coli* XGPRT and *E. coli* HPRT by the ANPs was tested. MDP (39 µM) and foscarnet (12 µM for wild type *E. coli* XGPRT and 29 µM for *E. coli* HPRT) did not inhibit these enzymes in the conditions that will be used to test the influence of PP_i on inhibition by the ANPs. In the assays with the ANP inhibitor, the concentration of foscarnet and MDP ranged from 38-39 µM and 12-29 µM, respectively, and was always higher than the concentration of the ANP inhibitor.

Inhibition of wild type *E. coli* XGPRT by phosphate was also tested. For this experiment, a 50 mM stock solution of phosphate buffer pH 7.4 was prepared. The assay consisted of 1 ml of assay buffer, 50 µM guanine, 243 or 602 µM of phosphate buffer, 425 µM *P*Rib-*PP* and 6.3 nM wild type *E. coli* XGPRT in a total cuvette volume of 1246 µl.

3.9. CRYSTALLIZATION

Aliquots of wild type *E. coli* XGPRT in 0.05 M Tris-HCl, 0.01 M $MgCl_2$, 1 mM DTT and pH 7.4 were concentrated to 19 mg/ml. The enzyme was crystallized with 1:0.98 stoichiometry of DR3876 by hanging drop vapor diffusion method at 18°C (Figure 3.1). The concentration of enzyme monomer in each hanging drop was 1.26 mM and the concentration of inhibitor was 1.24 mM. Two 96-well

hanging drop plates in a Mosquito® Crystal technology unit with 192 different conditions (from factorial screens from Wizard I, Wizard II and PEGIon) were used in search for conditions that led to crystallization of the inhibitor-bound enzyme. The Mosquito® Crystal technology has a variety of advantages over manual setup of crystallization experiments. First, this system requires much smaller volumes of sample. This is not really a problem for crystallization experiments for *E. coli* XGPRT as it is produced in large amounts e.g. 2 liters of cell culture produce around 100 mg of enzyme. Second, Mosquito® Crystal technology can rapidly screen 96 different conditions per screening plate. The setup for one such screening plate takes approximately 20 minutes as compared to the larger wells (manual setup) which can take up to two hours or more for 96 wells. Third, this system is fully automatic. The screening plates are housed in a temperature controlled (18°C) module which automatically takes pictures of the hanging drops at prescribed times, giving a step by step view of possibly developing crystals. Fourth, the automatic nature of this system as well as the use of new pipette tips for the preparation of each hanging drop guaranties no risk of cross-contamination.

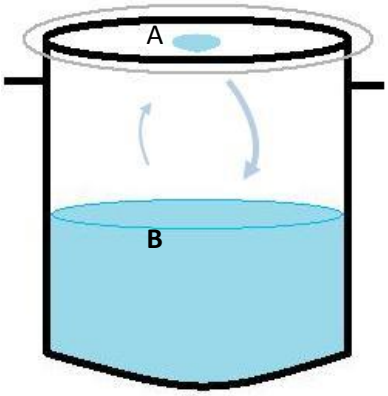

Figure 3.1. Hanging drop vapor diffusion method. Water vaporizes from the hanging drop (**A**) and transfers to the well solution (**B**) until equilibrium is reached and both solutions have the same concentration of buffer and precipitant. Grease is used to seal the glass lid on top off the well to prevent drying out of the drop and well solution.

The hanging drop vapor diffusion method involves a droplet containing (1) purified and concentrated protein (generally 20 mg/ml), (2) buffer and (3) precipitant. The hanging drop is allowed to equilibrate with a larger reservoir, the well solution, containing similar buffers and precipitants at higher concentrations. The content of the droplet is normally an equal amount of well solution and concentrated protein solution. Initially, the droplet contains an insufficient concentration of precipitant for crystallization, but as water vaporizes from the drop and transfers to the well solution, the precipitant concentration increases slowly to a level optimal for crystallization. The system must be sealed off from the outside using high-vacuum grease between the glass surfaces as both the droplet and well solution would dry out.

In the majority of screening experiments using Mosquito® Crystal technology, it is normal that only one or two crystals are obtained from over different 576 conditions. As crystals formed in the 96-well plates cannot be taken out to collect X-ray data from, large scale crystallization in bigger 24-well plates has to be undertaken. Thus, conditions in which crystals were formed in the 96-well screening plates, were manually repeated in these 24-well plates at 18°C and the hanging drop consisted of 1 µl of precipitant solution mixed together with 1 µl of protein-inhibitor solution. The well solution consisted of 1 ml of the same precipitant solution. For the preparation of the crystallization conditions, PEG 4000 was purchased from Hampton Research (Aliso Viejo, United States). All the other chemicals that were used for the setup of these conditions were purchased from Sigma-Aldrich (St. Louis, United States). In the next step, the concentration of the salt components and/or pH was changed to optimize crystallization conditions.

Mounting of the crystals and handling of the operating software for collection of the X-ray data was carried out by Prof. Luke Guddat. Studies are continuing to obtain (other) highly diffracting crystals and then to solve and refine the crystal structure.

3.10. PROTON NMR

Previous NMR studies have been directed to studying the movement of the mobile loop of *E. coli* XGPRT when substrates bind and products are released. In a preliminary experiment using proton NMR, chemical shifts were investigated on binding of the inhibitor.

Wild type *E. coli* XGPRT (200 µl) was dialyzed overnight in 0.01 M phosphate buffer, 0.012 M $MgCl_2$, pH 7.4 with 1 mM DTT, at 4°C. Activity and concentration of the enzyme was investigated using spectrophotometric assays under conditions described previously (sections 3.3 and 3.5).

NMR experiments were performed on a Bruker 900 NMR spectrometer (Karlsruhe, Germany) at 298K. The proton spectra of DR3876 alone and free wild type *E. coli* XGPRT were collected first. The NMR samples contained 150 µM of DR3876 and 5 % D_2O in water in a total volume of 635 µl and 150 µM (in terms of subunits) free enzyme and 5 % D_2O in dialysis buffer in a total volume of 630 µl, respectively. D_2O was purchased from Sigma (St. Louis, United States). Next, proton spectra of DR3876 in complex with *E. coli* XGPRT at concentration ratio's of 1:5, 2:5, 3:5, 4:5, 1:1 and 2:1 (inhibitor : enzyme) were acquired. One dimensional ^1H spectra of the region from 0 to 20 ppm were collected with an excitation null at the water resonance.

The NMR spectra were obtained and analyzed with the help of Prof. Ian Brereton and Dr. Greg Pierens.

4. RESULTS

4.1. CORRELATION BETWEEN $[E]_0$ and V_{max}

Correlation between $[E]_0$ and V_{max} was determined for wild type and loop-out *E. coli* XGPRT, prior to the determination of kinetic constants and K_i values. The R^2-value were 0.999 and 0.994, respectively, showing that, as expected, $[E]_0$ is proportional to V_{max}. The results are shown in Figure 4.1 and validate the assays for the determination of kinetic constants and K_i values.

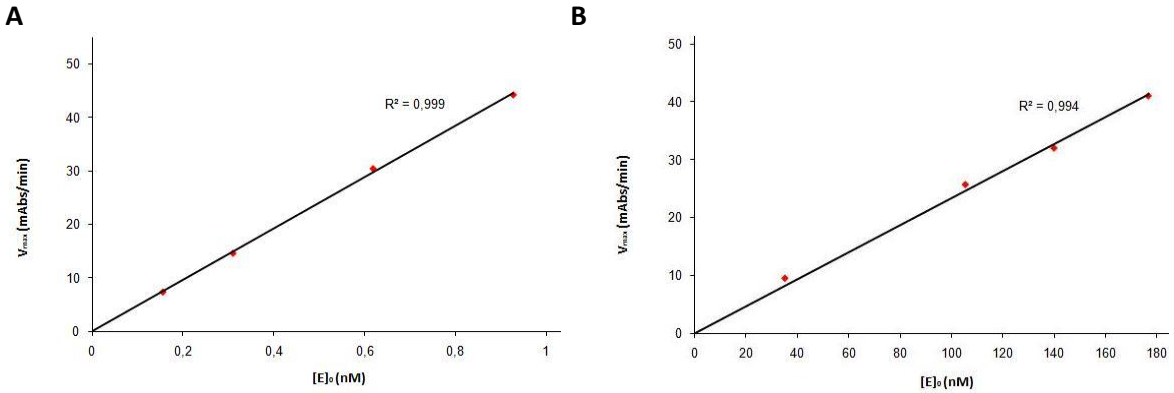

Figure 4.1. Correlation between $[E]_0$ and V_{max}. A The concentration of wild type *E. coli* XGPRT varied from 0.15 nM to 0.93 nM in terms of tetramer concentration. **B** Loop-out *E. coli* XGPRT concentrations varied from 35.2 nM to 176.7 nM in terms of tetramer concentration.

4.2. DETERMINATION OF KINETIC CONSTANTS FOR NATURALLY OCCURRING SUBSTRATES AND K_i VALUES FOR GMP

4.2.1. Determination of kinetic constants

Kinetic constants for the naturally occurring substrates for the three *E. coli* enzymes (wild type XGPRT, loop-out XGPRT and HPRT) were determined before commencing the study of the inhibitors. Hanes-Woolf plots were used to determine the kinetic constants (Addendum 1, Figures 1 to 3). The kinetic constants are shown in Table 4.1 and agree with those previously found in the literature.

Wild type and loop-out *E. coli* XGPRT have a preference for guanine and xanthine as purine substrates. The K_m values for *E. coli* loop-out XGPRT for guanine and *P*Rib-*PP* were similar to those for *E. coli* wild type XGPRT, confirming that binding of the substrates is not changed by removal of the mobile loop. For the wild type enzyme, the catalytic efficiency (k_{cat}/K_m values) for guanine and xanthine are 65-fold and 6-fold greater than the k_{cat}/K_m value for hypoxanthine, respectively (Table 4.1). For the loop-out enzyme, the k_{cat}/K_m values for guanine and xanthine are 130-fold and 7-fold greater than that for hypoxanthine, respectively. The k_{cat} for *P*Rib-*PP* for loop-out XGPRT is 150-fold lower than for wild type XGPRT, confirming previous results that the loop plays a role in the rate of catalysis.

Table 4.1. *Comparison of kinetic constants for the naturally occurring substrates for* E. coli *wild type XGPRT, loop-out XGPRT and HPRT*[a]

	$K_{m\ (app)}$ (μM)	k_{cat}[b] (s^{-1})	k_{cat}/K_m ($\mu M^{-1}\ s^{-1}$)
E. coli XGPRT (wild type)			
Guanine	2.6 ± 0.7	34.1 ± 2.7	13.1
*P*Rib-*PP*[c]	32.4 ± 3.2	28.2 ± 0.8	0.87
E. coli XGPRT (loop-out)			
Hypoxanthine	92.9 ± 40.5	0.024 ± 0.003	0.0003
Guanine	1.9 ± 0.2	0.073 ± 0.002	0.0384
Xanthine	33.2 ± 3.3	0.069 ± 0.003	0.0021
*P*Rib-*PP*[d]	28.3 ± 7.3	0.19 ± 0.02	0.0067
E. coli HPRT			
*P*Rib-*PP*[d]	45.9 ± 2.5	66.9 ± 1.2	1.46

[a] K_m values were measured in 0.1 M Tris-HCl, 0.012 M $MgCl_2$ at pH 7.40. [b] k_{cat} calculated in terms of the concentration of subunits with four active sites per molecule of enzyme. [c] Guanine as the 6-oxopurine base substrate. [d] Hypoxanthine as the 6-oxopurine base substrate.

4.2.2. K_i values for GMP

K_i values for GMP were determined for *E. coli* wild type XGPRT and loop-out XGPRT. Results were as previously found: GMP is a competitive inhibitor of both enzymes, and the K_i value for GMP was 10-fold lower for wild type *E. coli* XGPRT than for the loop-out mutant (Figure 4.2). This result confirms that the removal of the loop affects not only catalysis but that its presence is important for the binding of the nucleoside monophosphate products of the reaction.

Hanes-Woolf plots were used to determine the K_i values and are shown in Figure 4.2.

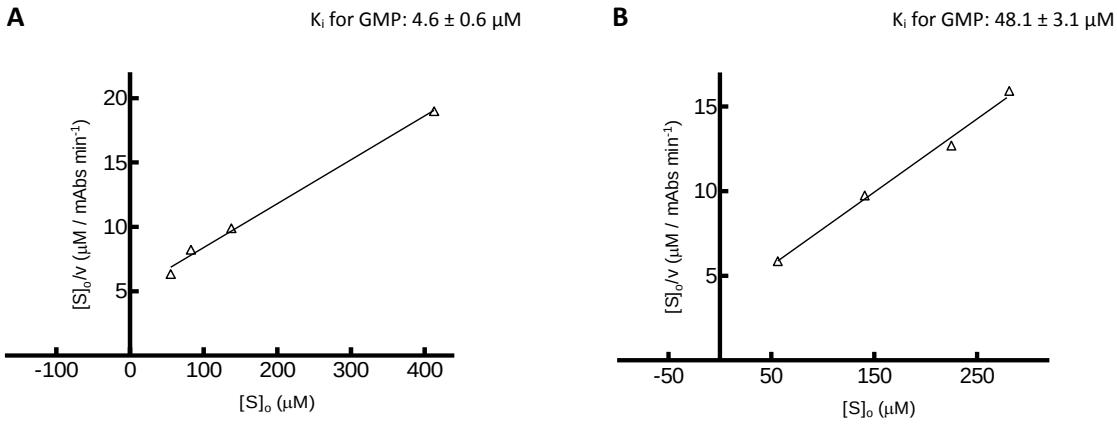

Figure 4.2. Hanes-Woolf plots for the determination of K_i values for GMP. The concentration of *P*Rib-*PP* is variable and the concentration of guanine is fixed at 47 μM. **A** Wild type *E. coli* XGPRT **B** Loop-out *E. coli* XGPRT.

4.3. DETERMINATION OF K_i VALUES FOR THE ANPs

4.3.1. DR3876

Initial rates for assays of the three *E. coli* enzymes under standard assay conditions in the presence and absence of DR3876 are shown in Figure 4.3. These rates were measured to determine the optimal concentration of the inhibitor to measure the K_i value.

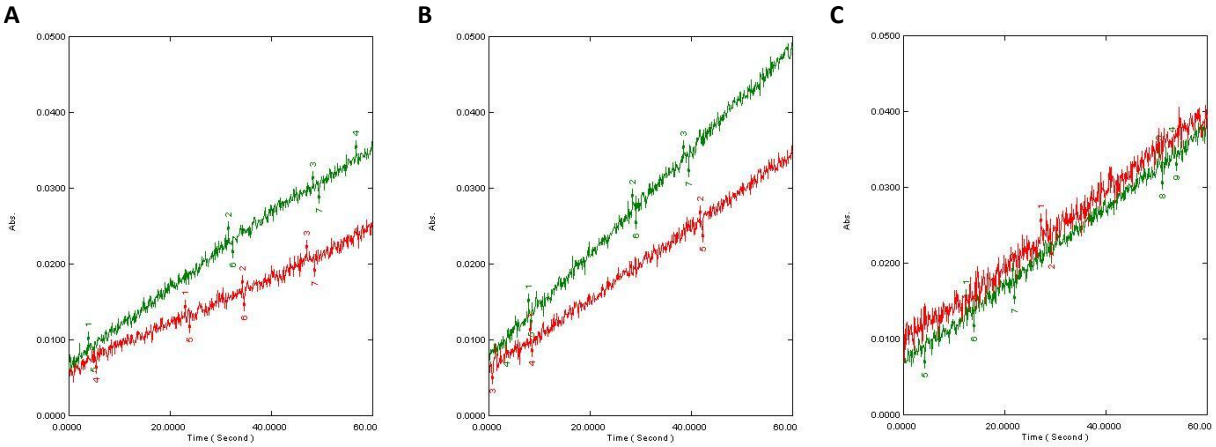

Figure 4.3. Assays of *E. coli* XGPRT (wild type and loop-out) and HPRT in presence (red) and absence (green) of DR3876. The concentration of 6-oxopurine base and *P*Rib-*PP* was 50 µM and 600 µM, respectively. **A** Wild type *E. coli* XGPRT in the presence or absence of DR3876 (0.8 µM). **B** Loop-out *E. coli* loop-out XGPRT in the presence or absence of DR3876 (4.4 µM). **C** *E. coli* HPRT in the presence or absence of DR3876 (8.6 µM).

The V_{max} was constant for both wild type and loop-out *E. coli* XGPRT and $K_{m\ (app)}$ increased from 32.4 ± 3.2 µM to 155.0 ± 17.1 µM for the wild type enzyme and from 28.3 ± 7.3 µM to 88.1 ± 15.2 µM for the loop-out mutant (Table 4.2). For the loop-out enzyme, the concentration of inhibitor was 5-fold higher than the concentration used to obtain inhibition of the wild type enzyme.

Table 4.2. *Kinetic constants for* E. coli *XGPRT (wild type and loop-out) in the presence of DR3876*

	[DR3876] (µM)	$K_{m\ (app)}$ (µM) *P*Rib-*PP*[b]	V_{max} (µM min^{-1})
E. coli XGPRT			
wild type	0.8	155.0 ± 17.1 (32.4 ± 3.2)	5.1 ± 0.2
loop-out	4.4	88.1 ± 15.2 (28.3 ± 7.3)	5.9 ± 0.3

[a] $[E]_0$ calculated in terms of concentration of subunits with four active sites per molecule of enzyme. [b] K_m values of *P*Rib-*PP* in the absence of inhibitor are shown in brackets.

At a maximum concentration of 8.6 µM of DR3876 able to be used in the spectrophotometric assay, no inhibition of *E. coli* HPRT was observed (Figure 4.3). This concentration is 10-fold higher than the concentration used to obtain inhibition for wild type XGPRT. Therefore, the K_i for DR3876 for *E. coli* HPRT was calculated to be >> 65 µM.

DR3876 inhibits *E. coli* wild type XGPRT with a K_i value of 0.23 ± 0.03 µM (Table 4.3). In comparison, there is a 10-fold difference between the K_i value for DR3876 for the wild type and loop-out enzyme, as found for GMP (Figure 4.2). However, DR3876 binds more tightly to these enzymes than GMP. The K_i values were calculated from the data in Table 4.2.

Table 4.3. *K_i values of DR3876 for* E. coli *wild type XGPRT, loop-out XGPRT and HPRT*

	K_i (µM)
E. coli XGPRT	
wild type	0.23 ± 0.03
loop-out	2.1 ± 0.4
E. coli HPRT	NI[a]

[a] NI = no inhibition. At a concentration of 8.6 µM of DR3876, no inhibition of *E. coli* HPRT was observed.

4.3.2. MK520

The effect of MK520 on the three *E. coli* enzymes is shown in Figure 4.4.

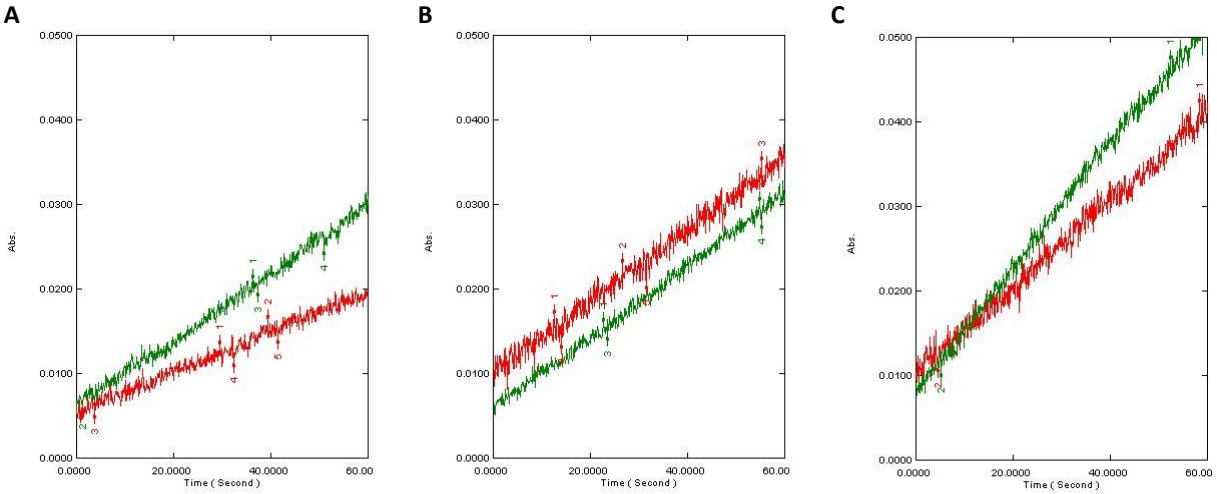

Figure 4.4. Assays of *E. coli* XGPRT (wild type and loop-out) and *E. coli* HPRT in the presence (red) and absence (green) of MK520. The concentration of 6-oxopurine base and *P*Rib-*PP* was 50 µM and 600 µM, respectively. **A** Wild type *E. coli* XGPRT in the presence or absence of MK520 (11.0 µM). **B** Loop-out *E. coli* XGPRT in the presence or absence of MK520 (32.1 µM). **C** *E. coli* HPRT in the presence or absence of MK520 (24.1 µM).

For wild type *E. coli* XGPRT, the V_{max} was constant and $K_{m\ (app)}$ increased from 32.4 ± 3.2 µM to 54.5 ± 7.1 µM (Table 4.4). This is consistent with competitive inhibition. For *E. coli* HPRT, the V_{max} decreased and the $K_{m\ (app)}$ increased from 45.9 ± 2.5 µM to 59.5 ± 5.4 µM (Table 4.4).

Table 4.4. *Kinetic constants for* E. coli *wild type XGPRT and* E. coli *HPRT in the presence of MK520*

	[MK520] (µM)	$K_{m\ (app)}$ (µM) *P*Rib-*PP*[a]	V_{max} (µM min^{-1})
wild type *E. coli* XGPRT	11.0	54.5 ± 7.1 (32.4 ± 3.2)	3.8 ± 0.1
E. coli HPRT	32.1	59.5 ± 5.4 (45.9 ± 2.5)	14.3 ± 0.4

[a] K_m values of *P*Rib-*PP* in the absence of inhibitor are shown in brackets.

For loop-out *E. coli* XGPRT, no inhibition was observed at a maximum concentration of 32.1 µM of MK520 (Figure 4.4). This was the highest concentration of inhibitor that could be added because of the limits of the spectrophotometric assay. This concentration is 3-fold higher than the concentration used to obtain good inhibition for wild type XGPRT. The K_i value for MK520 for loop-out *E. coli* XGPRT was calculated to be >> 118 µM, using equations (1) and (2). The K_i value for MK520 for *E. coli* wild type is shown in Table 4.5.

The K_i value for MK520 for *E. coli* HPRT is 73.2 ± 6.6 µM. The K_i value of MK520 is also lower for wild type *E. coli* XGPRT than for *E. coli* HPRT, as found for DR3876. K_i values of MK520 for the inhibition of *E. coli* HPRT were calculated for different substrate concentrations based on competitive inhibition (Equations (1) and (2)) (Table 4.6).

Table 4.5. *K_i values for MK520 for* E. coli *wild type XGPRT and loop-out XGPRT*

	K_i (µM)
E. coli XGPRT	
wild type	16.1 ± 2.1
loop-out	NI[a]

[a] NI = no inhibition. No inhibition of *E. coli* loop-out XGPRT was observed at a concentration of 32.1 µM of MK520.

Table 4.6. *Effect of substrate concentrations on K_i values of MK520 for inhibition of* E. coli *HPRT*

Concentration of *P*Rib-*PP*(µM)	K_i (µM) MK520[a]
393	8.2
262	8.6
131	16.6
79	17.9
52	25.6
26	26.6

[a] K_i calculated based on competitive inhibition using equations (1) and (2).

4.3.3. MK455

Inhibition of the three *E. coli* enzymes by MK455 is shown in Figure 4.5.

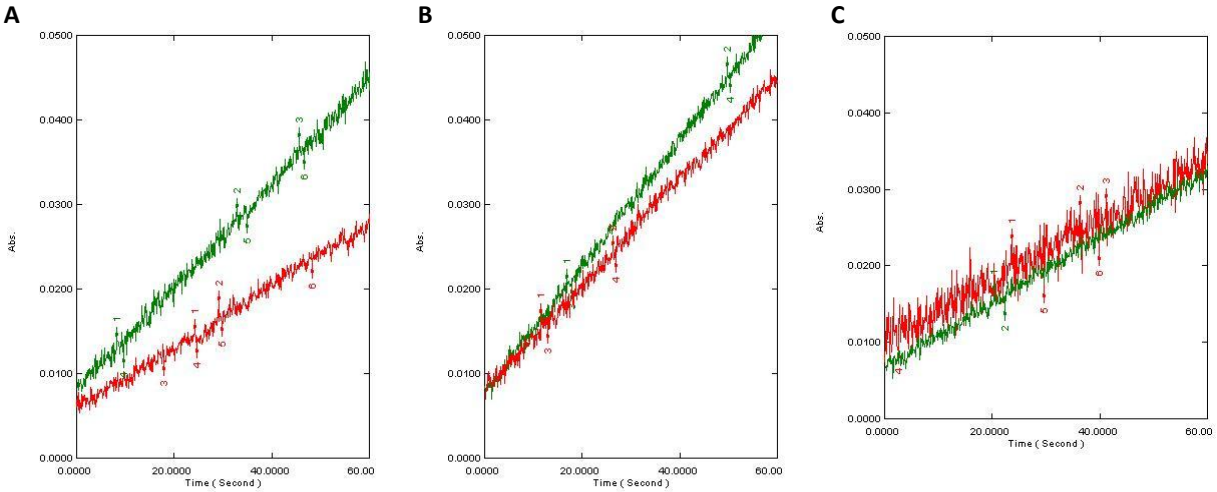

Figure 4.5. Assays of *E. coli* XGPRT (wild type and loop-out) and *E. coli* HPRT in the presence (red) and absence (green) of MK455. The concentration of 6-oxopurine base and *P*Rib-*PP* was 50 µM and 600 µM, respectively. **A** Wild type *E. coli* XGPRT ± MK455 (4.0 µM). **B** Loop-out *E. coli* XGPRT ± MK455 (7.7 µM). **C** *E. coli* HPRT ± MK455 (31.7 µM).

For wild type *E. coli* XGPRT, $K_{m\ (app)}$ increased from 32.4 ± 3.2 µM to 46.7 ± 4.8 µM and the V_{max} decreased (Table 4.7), showing that this compound is also not a competitive inhibitor with *P*Rib-*PP*.

Table 4.7. *Kinetic constants for* E. coli *XGPRT (wild type and loop-out) in the presence of MK455*

	[MK455] (µM)	$K_{m\ (app)}$ (µM) *P*Rib-*PP*[a]	V_{max} (µM min^{-1})
E. coli XGPRT			
wild type	4.0	46.7 ± 4.8 (32.4 ± 3.2)	4.1 ± 0.1
loop-out	7.7	28.9 ± 2.2 (28.3 ± 7.3)	5.9 ± 0.1

[a] K_m values of *P*Rib-*PP* in the absence of inhibitor are shown in brackets.

In the assay to determine the $K_{m\ (app)}$ for the loop-out enzyme, a concentration of 4.0 µM of MK455 was used. This concentration is lower than 7.7 µM as used in the previous experiment (Figure 4.5) due to the limited stock of MK455. The V_{max} was constant and $K_{m\ (app)}$ did not change (Table 4.7). Thus, at a concentration of 4.0 µM of MK455, there was no inhibition of the loop-out enzyme. This concentration is the same concentration used to obtain good inhibition for the wild type enzyme. The K_i for MK455 for *E. coli* loop-out XGPRT was calculated to be $\geq$ 3 µM.

Data obtained from the assay to determine the K_i value for MK455 for the wild type enzyme, showed that V_{max} for the wild type enzyme decreased. In a next step, inhibition of wild type *E. coli* XGPRT was investigated with different concentrations of MK455 and the K_i value was calculated based on competitive inhibition. The results from this assay are listed in Table 4.8.

Table 4.8. *K_i values of MK455 for* E. coli *wild type XGPRT based on competitive inhibition.*

[MK455]	K_i (µM)[a]
7.9 µM	0.4
3.9 µM	0.5

[a] K_i based on competitive inhibition and calculated using equations (1) and (2).

For *E. coli* HPRT, a maximum concentration of 31.7 µM of inhibitor only resulted in 11% inhibition (Figure 4.5). This concentration is 8-fold higher than the concentration used to obtain inhibition for wild type *E. coli* XGPRT. The K_i for MK455 for *E. coli* HPRT was calculated to be $\geq$ 700 µM.

Inhibition of *E. coli* HPRT was investigated with different concentrations of MK455 and the K_i value was calculated based on competitive inhibition. The results from this assay are listed in Table 4.9.

Table 4.9. *K_i values of MK455 for* E. coli *HPRT based on competitive inhibition.*

[MK455]	K_i (µM)[a]
7.9 µM	177
15.9 µM	357
23.8 µM	535
31.7 µM	700

[a] K_i based on competitive inhibition and calculated using equations (1) and (2).

4.4. EFFECT OF PP_i ON BINDING OF THE INHIBITORS

4.4.1. Effect of PP_i and structural analogs on the *E. coli* enzymes

ImmGP only binds human HGPRT in the presence of $Mg^{2+}.PP_i$ and there is evidence for a similar pyrophosphate binding pocket in the *E. coli* 6-oxopurine salvage enzymes. Therefore, the influence of PP_i and structural analogs of PP_i on inhibition of these enzymes by the ANPs was investigated. The structures of PP_i and its structural analogs, foscarnet and MDP, are presented in Figure 4.6.

A **B** **C**

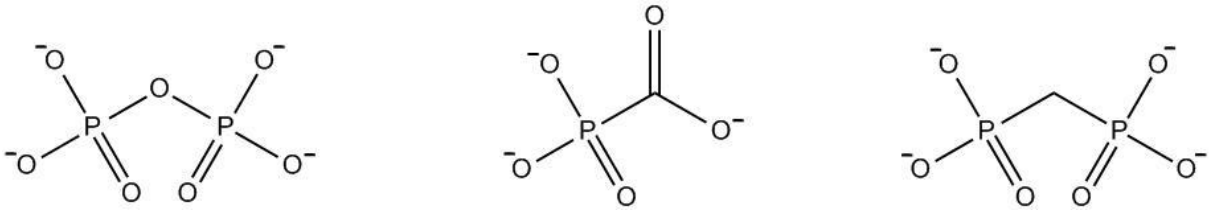

Figure 4.6. Structures of pyrophosphate, foscarnet and methylenediphosphonate. A Pyrophosphate. The P-O-P angle is 134.08°. **B** Foscarnet (currently used as an antiviral drug as it acts as a structural mimic of pyrophosphate). **C** Methylenediphosphonate. The P-C-P angle is 117.21°.

To ascertain that a change of inhibition of the enzyme was due to the ANPs and not because of inhibition by PP_i (or a structural analog), enzyme activities were measured for the enzymes in the absence of ANPs and in the presence of added PP_i, foscarnet and MDP. Foscarnet, PP_i and MDP did not inhibit wild type *E. coli* XGPRT and *E. coli* HPRT at the concentrations to be used to investigate their influence on inhibition by the ANPs. Results also showed that there is no inhibition of wild type *E. coli* XGPRT by concentrations of phosphate up to 602 µM. The influence of phosphate on the inhibition of the *E. coli* enzymes by the ANPs was not tested.

4.4.2. DR3876

Influence of PP_i and foscarnet on the inhibition by DR3876 was investigated for wild type *E. coli* XGPRT. The substrate concentrations (guanine and *P*Rib-*PP*) were saturated. However, foscarnet (1.2 µM) and PP_i (82.1 µM) did not affect inhibition by DR3876. Influence on the inhibition of DR3876 of loop-out *E. coli* XGPRT and *E. coli* HPRT was not investigated.

4.4.3. MK520

Influence of PP_i and foscarnet on the inhibition of wild type *E. coli* XGPRT by MK520 was investigated. Foscarnet (12 µM) and PP_i (33 µM) did not affect inhibition by MK520. Influence on the inhibition of loop-out *E. coli* XGPRT was not tested.

The effect of PP_i, foscarnet and MDP on the inhibition of *E. coli* HPRT by MK520 (27 µM) was investigated. At high substrate concentration (400 µM *P*Rib-*PP*), there was no influence of PP_i (33 µM), MDP (39 µM) or foscarnet (29 µM) on the inhibition of *E. coli* HPRT by MK520. However, at low substrate concentrations (<100 µM *P*Rib-*PP*) in the presence of PP_i (33 µM), there was an effect on the inhibition of the enzyme by MK520 (27 µM). The effect of foscarnet and MDP on the inhibition at low substrate concentrations was not investigated.

Because of the effect of PP_i on the inhibition of *E. coli* HPRT by MK520, the kinetic constants for MK520, in the presence of PP_i, were investigated (Table 4.10). The V_{max} decreased and K_m increased from 45.9 ± 2.5 to 63.9 ± 4.4 µM. The K_i value of MK520 in the presence of PP_i, was determined to be 71.8 ± 4.9 µM. Thus, the presence of PP_i had no effect on the inhibition.

Table 4.10. *Kinetic constants for* E. coli *HPRT in the presence of MK520 and presence or absence of PP_i.*

	$K_{m\,(app)}$ (µM) *P*Rib-*PP*	V_{max} (µM min^{-1})
In presence of 28 µM MK520 and 34 µM PP_i	63.9 ± 4.4	7.8 ± 0.1
In presence of 28 µM MK520 but absence of PP_i	59.5 ± 5.4	14.3 ± 0.4

K_i values of MK520 for the inhibition of *E. coli* HPRT were then calculated for different substrate concentrations based on the equation for competitive inhibition (Table 4.11).

Table 4.11. *Effect of substrate concentrations on K_i values of MK520 for inhibition of* E. coli *HPRT (in presence of PP_i)*[a]

Concentration of *P*Rib-*PP* (µM)	K_i (µM) MK520 + 34 µM of PP_i
407	5.2
272	7.0
136	10.5
81	15.0

[a] K_i calculated based on competitive inhibition using equations (1) and (2).

4.4.4. MK455

4.4.4.1. Wild type *E. coli* XGPRT

The effect of PP_i, foscarnet and MDP on the inhibition of wild type *E. coli* XGPRT by MK455 was investigated. In the presence of PP_i (33 µM), the inhibition of the enzyme by MK455 was increased from 40% to 65% (Figure 4.7).

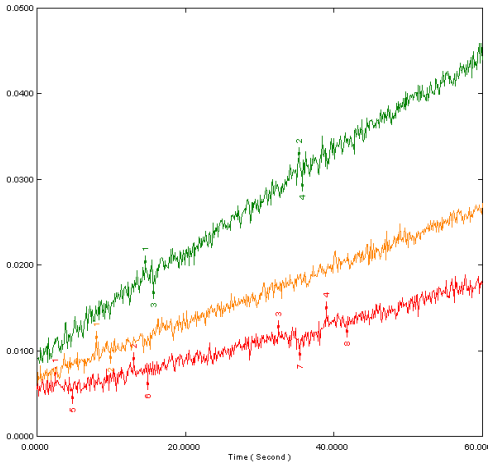

Figure 4.7. Effect of PP_i on the inhibition of wild type *E. coli* XGPRT by MK455. The concentration of the substrates, guanine and *P*Rib-*PP*, was 50 µM and 600 µM, respectively. Orange is in the presence of inhibitor and in the absence of PP_i. Red is in the presence of inhibitor and PP_i. The green line is in the absence of inhibitor and PP_i.

There was no effect of foscarnet (12 µM) or MDP (39 µM) on the inhibition of *E. coli* XGPRT by MK455 (4.0 µM).

Because of the effect of PP_i on the inhibition of the enzyme by MK455, the kinetic constants for MK455, in the presence of PP_i, were determined (Table 4.12). The V_{max} was constant and $K_{m\ (app)}$ increased from 32.4 ± 3.2 µM to 231.5 ± 8.7 µM. Thus, for MK455, the presence of PP_i affected the binding of the ANP so that it became competitive with *P*Rib-*PP*.

Table 4.12. *Kinetic constants for* E. coli *wild type XGPRT in the presence of MK455 and presence or absence of PP_i.*

	$K_{m\ (app)}$ (µM) *P*Rib-*PP*	V_{max} (µM min^{-1})
In presence of 2.0 µM MK455 and 33 µM PP_i	231.5 ± 8.7	5.3 ± 0.1
In presence of 2.0 µM MK455 but absence of PP_i	46.7 ± 4.8	4.1 ± 0.1

MK455, in the presence of PP_i, is a competitive inhibitor of wild type *E. coli* XGPRT with a K_i value of 0.32 ± 0.01 µM.

4.4.4.2. Loop-out *E. coli* XGPRT

The effect of PP_i on the inhibition of loop-out XGPRT by MK455 was investigated. The concentration of MK455 was 4.1 µM (lower than 7.7 µM as used in the previous experiment due to the limited stock of MK455) and the concentration of PP_i was 34.1 µM. The V_{max} was constant and $K_{m(app)}$ did not change (Table 4.13).

Table 4.13. *Kinetic constants for* E. coli *loop-out XGPRT in the presence of MK455 and presence or absence of PP_i.*

	$K_{m\ (app)}$ (μM) *P*Rib-*PP*	V_{max} (μM min^{-1})
In presence of 4.1 μM MK455 and 34.1 μM PP_i	29.7 ± 6.9	6.4 ± 0.4
In presence of 4.1 μM MK455 but absence of PP_i	28.9 ± 2.2	5.9 ± 0.1

Thus, at a concentration of 4.1 μM of MK455 in the presence of 34.1 μM PP_i, there was no inhibition of the loop-out enzyme. This concentration is 2-fold higher than the concentration used to obtain good inhibition for the wild type enzyme (in the presence of PP_i). The K_i for MK455 in the presence of PP_i, for loop-out *E. coli* XGPRT was calculated to be $\geq$ 3 μM. This K_i value is 10-fold higher than for the wild type enzyme in the presence of PP_i, supporting previous results that there is more affinity of the ANPs for the wild type than for the loop-out enzyme.

4.4.4.3. *E. coli* HPRT

The effect of PP_i on the inhibition of *E. coli* HPRT by MK455 was also investigated (Figure 4.8). The V_{max} was constant and $K_{m\ (app)}$ increased from 12.5 ± 2.4 μM to 77.6 ± 9.0 μM (Table 4.14). The K_i for MK455 in the presence of PP_i, for *E. coli* HPRT was calculated to be 35.2 ± 4.1 μM.

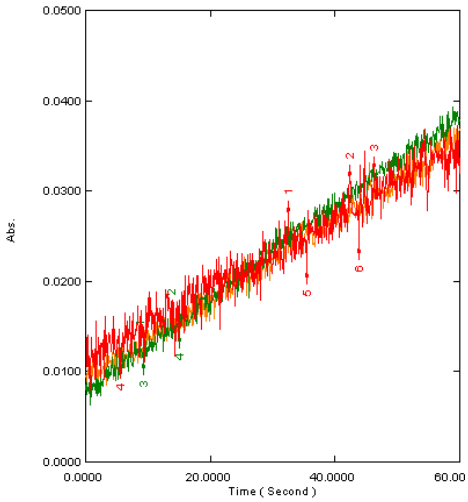

Figure 4.8. Effect of PP_i on the inhibition of *E. coli* HPRT by MK455. Orange is in the presence of inhibitor and the absence of PP_i. Red is in the presence of inhibitor and PP_i. The green line is in the absence of inhibitor and PP_i.

Table 4.14. *Kinetic constants for* E. coli *HPRT in the presence of MK455 and PP_i.*

	$K_{m\ (app)}$ (μM) *P*Rib-*PP*	V_{max} (μM min^{-1})
In presence of 24.3 μM MK455 and 34 μM PP_i	77.6 ± 9.0	23.2 ± 0.9

4.5. CRYSTALLIZATION OF DR3876-BOUND *E. coli* XGPRT

Two 96-well plates with screening conditions for crystallization were tested and crystals were quickly (12-36 hours) visible in various conditions and reached their maximum size within a week. Most of the conditions that produced crystals are listed in Table 4.15. Photographs of crystals of *E. coli* XGPRT in the presence of DR3876 are shown in Figure 4.9.

Table 4.15. *Crystallization conditions for wild type* E. coli *XGPRT in the presence of DR3876*[a]

1.	20% (w/v) PEG 3350, 0.2 M sodium malonate
2.	12% (w/v) PEG 3350, 0.1 M sodium malonate
3.	20% (w/v) PEG 3350, 8% tacsimate[b] (crystals were formed in pH6, pH7 and pH8)
4.	20% (w/v) PEG 3350, 0.2 M sodium formate
5.	20% (w/v) PEG 3350, 0.2 M ammonium citrate
6.	20% (w/v) PEG 3350, 0.2 M citric acid
7.	20% (w/v) PEG 3350, 0.2 M lithium citrate
8.	20% (w/v) PEG 3350, 0.2 M potassium sodium tartrate
9.	20% (w/v) PEG 3350, 0.2 M lithium nitrate
10.	20% (w/v) PEG 3350, 0.2 M potassium thiocyanate
11.	20% (w/v) PEG 3350, 0.2 M sodium chloride
12.	30% (w/v) PEG 400, 0.1 M Tris (pH 8.5), 0.2 M magnesium chloride
13.	0.1 M sodium acetate (pH 4.5), 0.8 M sodium phosphate, 1.2 M potassium phosphate
14.	0.2 M lithium sulfate, 1.0 M potassium sodium tartrate, 0.1 M Tris (pH 7.0)

[a] The crystallization conditions were obtained from factorial screens Wizard I, Wizard II and PEGIon achieved from Emerald Biosystems.

[b] Tacsimate is composed of a mixture of titrated organic acid salts and contains 1.8M malonic acid, 0.25M ammonium citrate tribasic, 0.12M succinic acid, 0.3M malic acid, 0.4M sodium acetate trihydrate, 0.5M sodium formate and 0.16M ammonium tartrate dibasic.

A **B**

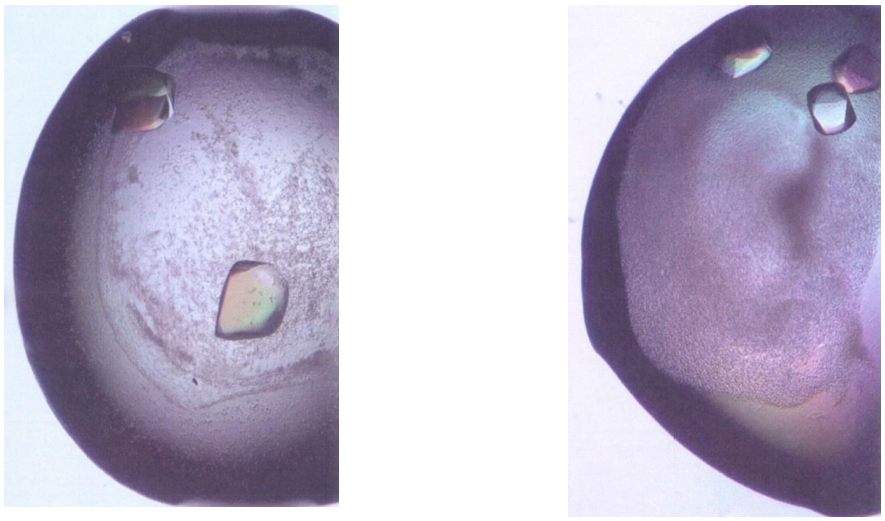

Figure 4.9. Photographs of DR3876-bound *E. coli* XGPRT crystals. A Crystals formed in 20% (w/v) PEG 3350 and 0.2 M sodium malonate (picture taken after 96 hours). **B** Crystals formed in 12% (w/v) PEG 3350, 0.1 M sodium malonate (picture taken after 60 hours).

Crystals formed in 20% (w/v) PEG 3350, 8% tacsimate, pH 6.0 (table 4.15, condition nr. 3) grew fast and maximum size was reached within 5 days. These were the largest crystals obtained from the screening plate. Pictures of the crystals at various moments in time are shown in Addendum 2.

Although a large number of relatively large and well-shaped crystals could be obtained, there was no guarantee that these crystals would diffract highly. Around 20 crystals were mounted by Prof. Luke Guddat but these all diffracted to ± 5 Å.

Crystals formed in 0.2 M lithium sulfate, 1.0 M potassium sodium tartrate and 0.1 M Tris (pH 7.0) (table 4.15, condition nr. 14) grew reproducibly in large 24-well plates. Crystallization data from these inhibitor-bound *E. coli* XGPRT crystals were measured to a resolution of 2.9 Å by Professor Luke Guddat but results have yet to be refined. However, it was possible to confirm that the inhibitor is bound in the active site.

4.6. PROTON NMR

Proton spectra of free *E. coli* XGPRT, free DR3876 and DR3876-bound *E. coli* XGPRT were obtained. The proton spectrum of DR3876-bound *E. coli* XGPRT is shown in Figure 4.10.

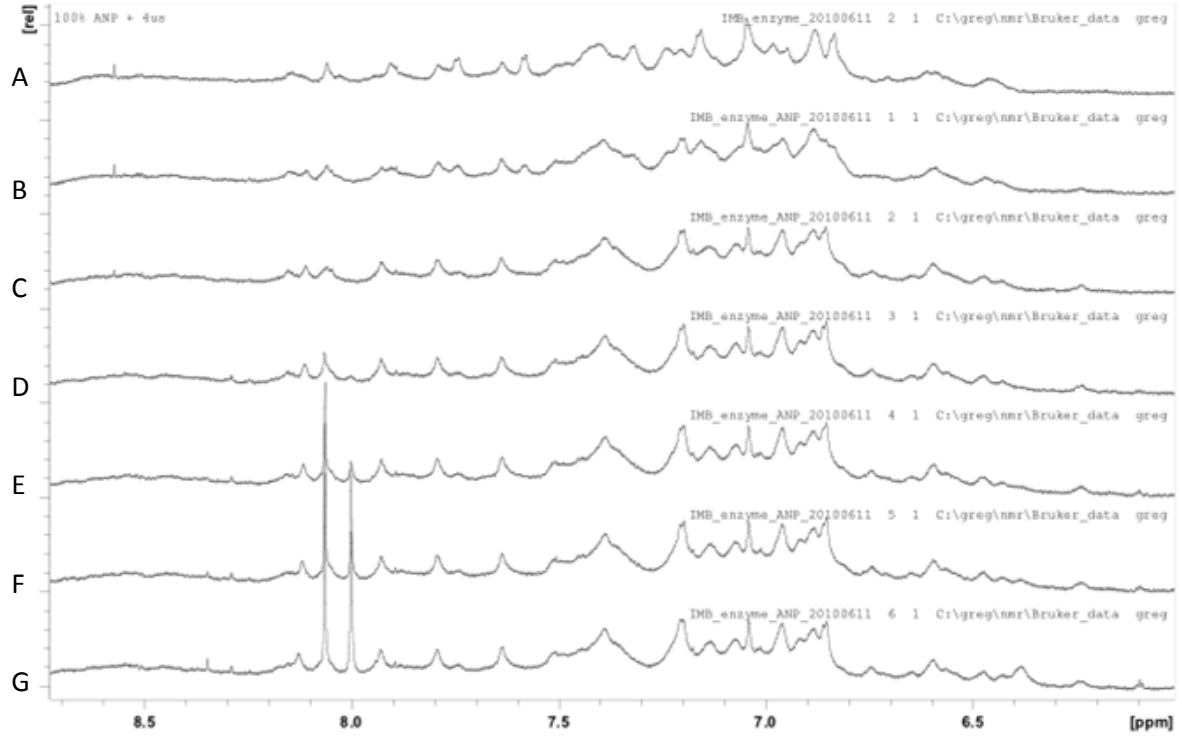

Figure 4.10. Proton NMR spectra of DR3876-bound *E. coli* XGPRT. Enzyme:ANP concentration ratio of the obtained spectra is **A.** pure enzyme **B.** 5:1 **C.** 5:2 **D.** 5:3 **E.** 5:4 **F.** 1:1 **G.** 1:2. Changes in the spectra can be observed at 6.60, 6.75, 6.96, 7.20, 7.30, 7.65, 8.00 and 8.08 ppm.

In this preliminary experiment using proton NMR, chemical shifts were observed on binding of DR3876. The assignment of these shifts awaits further experimentation. For now, changes can be observed in the peaks at 6.60, 6.75, 7.65, 8.00, 8.08 ppm (increasing peak volume) and in the peaks at 7.30 ppm (decrease in peak volume) and 6.96 and 7.20 ppm (two separate peaks merge into one single peak).

5. DISCUSSION

The first experiment, showing that $[E]_0$ is proportional to V_{max}, validates the assays for determination of the kinetic constants and K_i values. Results from the determination of kinetic constants for naturally occurring substrates (and K_i values for GMP) agreed with those previously found in the literature and ratify that kinetic constants and K_i values of the ANPs can be determined with satisfactory accuracy and precision. Discussion of the inhibition of the *E. coli* enzymes by these ANPs is provided below.

5.1. DR3876

DR3876 is a competitive inhibitor of wild type *E. coli* XGPRT with a K_i value 20-fold lower than that of GMP (K_i DR3876 = 0.23 ± 0.03 μM; K_i GMP = 4.6 ± 0.6 μM). Thus, replacement of the ribose ring by the alkoxyalkyl group and the phosphate group by a phosphonate moiety has a significant effect on the affinity for the active site. The fact that it is a competitive inhibitor with *P*Rib-*PP* shows that this compound very probably binds in the same position as GMP, the nucleoside monophosphate product of the reaction. The addition of $Mg^{2+}.PP_i$ did not increase inhibition of *E. coli* XGPRT by DR3876, as would be expected from previously found results where ImmGP only inhibits human HGPRT in the presence of $Mg^{2+}.PP_i$.

The removal of the flexible loop from wild type *E. coli* XGPRT, increases the K_i for DR3876 by a factor of 10-fold (K_i DR3876 = 2.1 ± 0.4 μM). This is the same factor as found for the K_i values for GMP between the wild type and loop-out enzyme (K_i GMP = 48.1 ± 3.1 μM). Therefore, this flexible loop plays a role not only in catalysis (a 470-fold decrease in k_{cat}; Table 4.1) but also in the binding of the ANPs and the nucleoside monophosphates. However, the loop is not involved in the binding of the two substrates, purine base or *P*Rib-*PP*, as these K_m values are unaffected (Table 4.1). This is presumably because the two substrates bind when the loop is in the open position and interactions between the amino acid side chains or the backbone atoms from the loop are not necessary for their binding in the active site. The difference in the affinity between the ANPs and the nucleoside 5'-monophosphate products of the reaction for these two enzymes could be attributed to the fact that, in the case of the nucleoside 5'-monophosphates, the loop is opening to release the product of the reaction (Figure 1.5). The ANPs are presumably anchored more tightly, as is reflected in their lower K_i values, and the loop is partially closed. This can be seen as the loop is well ordered and visible in the structure of human HGPRT with PEEG bound and neither ordered or visible in the structure of human HGPRT with GMP bound (Figure 1.5).

DR3876 does not inhibit *E. coli* HPRT at the maximum concentration used (8.6 µM). This could be partially attributed to the fact that, though guanine is a poor substrate for *E. coli* HPRT, there is a secondary effect in that the nucleoside monophosphates (GMP and IMP) also bind weakly (Table 1.2). However, given the fact that DR3876 binds to *E. coli* XGPRT with a K_i value 20-fold lower than for GMP, it could be predicted that his may be the same effect for *E. coli* HPRT. Thus, the predicted K_i value would be of the order of 53 µM, which can be measured accurately. Therefore, as no inhibition was observed, it could be concluded that this phosphonate tail precludes binding of the ANP to *E. coli* HPRT. This finding illustrates the difference in the active site between *E. coli* XGPRT and *E. coli* HPRT and demonstrates that the combination of the purine base (guanine) and the phosphonate moiety does not allow DR3876 to bind well in the active site.

Table 5.1. *Comparison of K_i values for DR3876, MK520 and MK455 for* E. coli *XGPRT (wild type and loop-out) and* E. coli *HPRT.* [a]

		K_i (µM)		
	purine base	wild type *E. coli* XGPRT	loop-out *E. coli* XGPRT	*E. coli* HPRT
DR3876	guanine	0.23 ± 0.03 (competitive)	2.1 ± 0.4 (competitive)	NI[b]
MK520	hypoxanthine	16.1 ± 2.1 (competitive)	NI[b]	73.2 ± 6.6 (not competitive)
MK455	guanine	0.4 [c] (not competitive)	≥ 3 [c]	≥ 700 [c]
MK520 in presence of PP_i	hypoxanthine	ND[d]	ND[d]	71.8 ± 4.9 (not competitive)
MK455 in presence of PP_i	guanine	0.32 ± 0.01 (competitive)	≥ 3 [b]	35.2 ± 4.1 (competitive)

[a] This table is a compilation of Tables 4.3, 4.5, 4.8 and 4.9.
[b] NI = no inhibition.
[c] K_i calculated based on competitive inhibition using equations (1) and (2).
[d] ND = not determined.

5.2. MK520 AND MK455

MK520 (hypoxanthine as purine base) and MK455 (guanine as purine base) were chosen for this study, as they have the same phosphonate tail and the only difference is the purine base. Therefore, knowing that *E. coli* XGPRT favors guanine and *E. coli* HPRT favors hypoxanthine, this difference allows a direct comparison of the effect of the purine base in the affinity. Thus, it could be predicted that MK520 may bind more tightly to *E. coli* HPRT compared to *E. coli* XGPRT and that MK455 would bind more tightly to *E. coli* XGPRT. As found for other ANPs for *P. falciparum* HGXPRT, *P. vivax* HGPRT and human HGPRT, the effect of the purine base and the phosphonate moiety can be additive, synergistic or they can negate each other. However, the binding of these two ANPs does not always obey strict competitive inhibition and is more complex than for DR3876.

For this phosphonate tail, when guanine is the purine base, the binding to wild type *E. coli* XGPRT is not competitive and, when hypoxanthine is the purine base, the binding to *E. coli* HPRT is not competitive. Thus, for this phosphonate tail, the attachment of the preferred purine base doesn't give competitive inhibition.

MK520, with hypoxanthine as the purine base, is a competitive inhibitor of wild type *E. coli* XGPRT though its K_i is high (16.1 ± 2.1 μM; Table 4.6). This is not unexpected since hypoxanthine is not the preferred base for this enzyme (Table 4.1). The surprising finding is that, when hypoxanthine is replaced by the preferred base, guanine (MK455), this compound becomes a not competitive inhibitor (Table 4.8). However, at maximum substrate concentrations and using the equation for competitive inhibition, MK455 is a very good inhibitor indeed with a calculated K_i value of 0.4 μM. When PP_i is added, strict competitive inhibition is observed and the K_i for MK455 is 0.32 ± 0.01 μM. Therefore, the combination of the preferred purine base, the phosphonate tail and PP_i, makes this compound an effective inhibitor. The effect of PP_i may be to orientate MK455 in the correct position in the active site.

Both MK520 and MK455 are weak inhibitors of the loop-out enzyme, reinforcing the proposition that the flexible loop has a crucial function in the binding of the ANPs. Even the combination of the preferred guanine base in MK455 and PP_i leads to weak inhibition of the loop-out enzyme. These data support the hypothesis that when the ANPs bind the flexible loop partially closes over the active site and that this loop movement is necessary to achieve low K_i values.

For *E. coli* HPRT, when the preferred base (hypoxanthine; MK520) is attached to the phosphonate tail, the inhibition is not competitive. The data in Table 4.7 and 4.12 suggests that MK520 is binding *E. coli* HPRT in the active site in such a way that it inhibits the naturally occurring substrates from binding, but not in a completely competitive way. These results indicate that inhibition of the enzyme by MK520, is mixed. The addition of PP_i did not affect this mode of binding. It is only when the purine base is guanine (MK455) and, in the presence of PP_i, that the inhibition is competitive and the ANP binds to the enzyme with an affinity 15-fold higher than for the corresponding nucleoside monophosphate, GMP.

5.3. DIFFERENT EFFECT OF PP_i AND MDP ON INHIBITION BY MK455

Inhibition of wild type *E. coli* XGPRT by MK455 is not competitive and when PP_i is added, strict competitive inhibition is observed. However, there was no influence of MDP on the inhibition of *E. coli* XGPRT by MK455 (section 4.4.3.1). This is surprising, considering the structural analogy between PP_i and MDP. An explanation of these results could be that the angle between the phosphorus atoms in the structure of PP_i and MDP is different (Figure 4.6).

The angle between P-O-P in ImmGP.Mg^{2+}.PP_i bound to human HGPRT is 134.08° (angle calculated in MarvinView using Protein Data Bank accession code 1bzy; *Shi et al., 1999*). The angle between P-C-P in MDP, in a free state, is 117.21° (*DeLaMatter et al., 1972*). The difference in angle between the two phosphorus atoms and the central atom, can explain the different characteristics these two compounds have when interacting with the enzyme. The change in angle results in a change of distance between the two phosphorus atoms (and the oxygen atoms that are bound to these phosphorus atoms). Due to this difference, it could be possible that MDP is not able to bind the pyrophosphate binding pocket in the same conformation PP_i does and therefore cannot interact with the ANP to make inhibition strictly competitive.

5.4. CRYSTALLIZATION AND PROTON NMR

In the majority of cases, it is normal that only one or two conditions giving crystals are found in screening large numbers of factorials. The obtained crystallization results show that, compared to most other proteins, *E. coli* XGPRT crystallizes easy and under many conditions. However, obtaining crystals does not mean that they will diffract highly or that their structures can be solved. Thus, though *E. coli* XGPRT does crystallize because of its very tight structure (*Vos et al., 1997*) and because it is a relatively small protein (molecular mass of a wild type *E. coli* XGPRT subunit is 16 805 daltons), structures of the enzyme in complex with an ANP inhibitor can still be a long way off. The hurdles involved in obtaining crystal structures are illustrated in Figure 5.1.

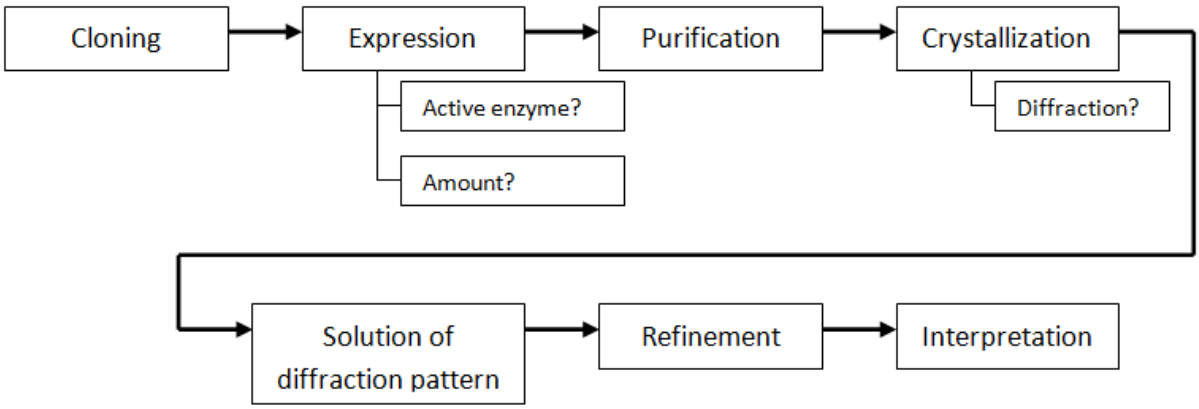

Figure 5.1. Diagram of difficulties involved in obtaining a crystal structure. Cloning of the cDNA coding for the desired enzyme is the first hurdle that needs to be taken. Expression of active enzyme in acceptable amounts and purification are the following obstacles. Obtaining highly diffracting crystals of the enzyme is the next hurdle. Additionally, solution of the diffraction pattern and structure refinement need to be completed. The final difficulty is interpretation of the acquired data.

Although structure solution and refinement were not yet carried out, it was possible to confirm that the inhibitor is bound in the active site. Only after the crystal structure of this complex is solved, it will be possible to determine specific interactions between the ANP inhibitor and *E. coli* XGPRT.

Proton NMR spectra of free *E. coli* XGPRT and in presence of increasing concentrations of DR3876, demonstrate that chemical shifts can be observed in the enzyme and these are attributed to the binding of the inhibitor. However, the resonances have not yet been assigned. These preliminary results could be the first step to more complex experiments, such as labeling of amino acid residues of the enzyme (for example some of the residues that form the flexible loop).

5.5. CONCLUSION

The three ANPs studied here (DR3876, MK520 and MK455) are good inhibitors of *E. coli* XGPRT and HPRT, but with widely different K_i values. These values depend on the nature of the purine base attached and the chemical structure of the linker between the base and the invariable phosphonate group. The flexible loop which closes over the active site of these enzymes during catalysis, plays a role in the affinity of the ANPs for these enzymes.

Crystals of *E. coli* XGPRT in complex with DR3876 have been obtained. The crystallization will now require optimization to produce highly diffracting crystals which allows for the specific interactions between the amino acid backbone and side chains and the inhibitor in the active site to be identified.

ANPs are known inhibitors of *P. falciparum* and *P. vivax* and the interactions between the investigated ANPs and the *E. coli* enzymes can contribute to the understanding of how these inhibitors interact with their target enzymes. In this way, the data presented in this thesis could assist in the search for enhanced drug leads.

6. REFERENCES

Balendiran, G.K.; Molina, J.A.; Xu, Y.; Torres-Martinez, J.; Stevens, R.; Focia, P.J.; Eakin, A.E.; Sacchettini, J.C.; Craig, S.P. 3rd (1999). Ternary complex structure of human HGPRTase, PRPP, Mg^{2+}, and the inhibitor HPP reveals the involvement of the flexible loop in substrate binding. *Protein Sci*, 8, 1023-31.

Benson, C.E.; Love, S.H.; Remy, C.N. (1970). Inhibition of *de novo* purine biosynthesis and interconversion by 6-methylpurine in *Escherichia coli. J Bacteriol,* 101, 872-80.

Biazus, G.; Schneider, C.Z.; Palma, M.S.; Basso, L.A.; Santos, D.S. (2009). Hypoxanthine-guanine phosphoribosyltransferase from *Mycobacterium tuberculosis* H37Rv: cloning, expression, and biochemical characterization. *Protein Expr Purif*, 66, 185-90.

Breman, J.G. (2009). Eradicating malaria. *Sci Prog*, 92, 1-38.

Carlton, J. (2003). The *Plasmodium vivax* genome sequencing project. *Trends Parasitol,* 19, 227-31.

Chalker, A.F.; Minehart, H.W.; Hughes, N.J.; Koretke, K.K.; Lonetto, M.A.; Brinkman, K.K.; Warren, P.V.; Lupas, A.; Stanhope, M.J.; Brown, J.R.; Hoffman, P.S. (2001). Systematic identification of selective essential genes in *Helicobacter pylori* by genome prioritization and allelic replacement mutagenesis. *J Bacteriol,* 183, 1259-68.

Cooke, E.M. (1985). *Escherichia coli*--an overview. *J Hyg (Lond)*, 9, 523-30.

Craig, S.P. 3rd; Eakin, A.E. (2000). Purine phosphoribosyltransferases. *J Biol Chem*, 275, 20231-4.

De Clercq, E.; Holý, A.; Rosenberg, I.; Sakuma, T.; Balzarini, J.; Maudgal, P.C. (1986). A novel selective broad-spectrum anti-DNA virus agent. *Nature*, 323, 464-7.

De Clercq, E.; Sakuma, T.; Baba, M.; Pauwels, R.; Balzarini, J.; Rosenberg, I.; Holý, A. (1987). Antiviral activity of phosphonylmethoxyalkyl derivatives of purine and pyrimidines. *Antiviral Res*, 8, 261-72.

De Gregorio, L.; Nyhan, W.L.; Serafin, E.; Chamoles, N.A. (2000). An unexpected affected female patient in a classical Lesch-Nyhan family. *Mol Genet Metab*, 69, 263-8.

Deo, S.S.; Tseng, W.C.; Saini, R.; Coles, R.S.; Athwal, R.S. (1985). Purification and characterization of *Escherichia coli* xanthine-guanine phosphoribosyltransferase produced by plasmid pSV2gpt. *Biochim Biophys Acta*, 839, 233-9.

Deutsch, S.I.; Long, K.D.; Rosse, R.B.; Mastropaolo, J.; Eller, J. (2005). Hypothesized deficiency of guanine-based purines may contribute to abnormalities of neurodevelopment, neuromodulation, and neurotransmission in Lesch-Nyhan syndrome. *Clin Neuropharmacol*, 28, 28-37.

Downie, M.J.; Saliba, K.J.; Howitt, S.M.; Bröer, S.; Kirk, K. (2006). Transport of nucleosides across the *Plasmodium falciparum* parasite plasma membrane has characteristics of *Pf*ENT1. *Mol Microbiol*, 60, 738-48.

Duckworth, M.; Ménard, A.; Megraud, F.; Mendz, G.L. (2006). Bioinformatic analysis of *Helicobacter pylori* XGPRTase: a potential therapeutic target. *Helicobacter*, 11, 287-95.

Eads, J.C.; Scapin, G.; Xu, Y.; Grubmeyer, C.; Sacchettini, J.C. (1994). The crystal structure of human hypoxanthine-guanine phosphoribosyltransferase with bound GMP. *Cell*, 78, 325-34.

Elgemeie, G.H. (2003). Thioguanine, mercaptopurine: their analogs and nucleosides as antimetabolites. *Curr Pharm Des*, 9, 2627-42.

Free, M.L.; Gordon, R.B.; Keough, D.T.; Beacham, I.R.; Emmerson, B.T.; de Jersey, J. (1990). Expression of active human hypoxanthine-guanine phosphoribosyltransferase in *Escherichia coli* and characterisation of the recombinant enzyme. *Biochim Biophys Acta*, 1087,205-11.

Gardner, M.J.; Hall, N.; Fung, E.; White, O.; Berriman, M.; Hyman, R.W.; Carlton, J.M.; Pain, A.; Nelson, K.E.; Bowman, S.; Paulsen, I.T.; James, K.; Eisen, J.A.; Rutherford, K.; Salzberg, S.L.; Craig, A.; Kyes, S.; Chan, M.S.; Nene, V.; Shallom, S.J.; Suh, B.; Peterson, J.; Angiuoli, S.; Pertea, M.; Allen, J.; Selengut, J.; Haft, D.; Mather, M.W.; Vaidya, A.B.; Martin, D.M.; Fairlamb, A.H.; Fraunholz, M.J.; Roos, D.S.; Ralph, S.A.; McFadden, G.I.; Cummings, L.M.; Subramanian, G.M.; Mungall, C.; Venter, J.C.; Carucci, D.J.; Hoffman, S.L.; Newbold, C.; Davis, R.W.; Fraser, C.M.; Barrell, B. (2002). Genome sequence of the human malaria parasite *Plasmodium falciparum*. *Nature*, 419, 498-511.

Giacomello, A.; Salerno, C. (1978). Human hypoxanthine-guanine phosphoribosyltransferase. Steady state kinetics of the forward and reverse reactions. *J Biol Chem*, 253, 6038-44.

Gots, J.S.; Benson, C.E. (1973). Genetic control of bacterial purine phosphoribosyltransferases and an approach to gene enrichment. *Adv Exp Med Biol*, 41, 33-9.

Griffin, P.M.; Ostroff, S.M.; Tauxe, R.V.; Greene, K.D.; Wells, J.G.; Lewis, J.H.; Blake, P.A. (1988). Illnesses associated with *Escherichia coli* O157:H7 infections. *Ann Intern Med*, 109, 705-12.

Guddat, L.W.; Vos, S.; Martin, J.L.; Keough, D.T.; de Jersey, J. (2002). Crystal structures of free, IMP-, and GMP-bound *Escherichia coli* hypoxanthine phosphoribosyltransferase. *Protein Sci*, 11, 1626-38.

Hanes, C.S. (1932). Studies on plant amylases: The effect of starch concentration upon the velocity of hydrolysis by the amylase of germinated barley. *Biochem J*, 26, 1406-21.

Holden, J.A.; Kelley, W.N. (1978). Human hypoxanthine-guanine phosphoribosyltransferase. Evidence for tetrameric structure. *J Biol Chem*, 253, 4459-63.

Jones, T.A.; Zou, J.Y.; Cowan, S.W.; Kjeldgaard, M. (1991). Improved methods for building protein models in electron density maps and the location of errors in these models. *Acta Crystallogr*. A47, 110–119.

Keough, D.T.; McConachie, L.A.; Gordon, R.B.; de Jersey, J.; Emmerson, B.T. (1987). Human hypoxanthine-guanine phosphoribosyltransferase. Development of a spectrophotometric assay and its use in detection and characterization of mutant forms. *Clin Chim Acta,* 163, 301-8.

Keough, D.T.; Ng, A.L.; Winzor, D.J.; Emmerson, B.T.; de Jersey, J. (1999). Purification and characterization of *Plasmodium falciparum* hypoxanthine-guanine-xanthine phosphoribosyltransferase and comparison with the human enzyme. *Mol Biochem Parasitol*, 98, 29-41.

Keough, D.T.; Skinner-Adams, T.; Jones, M.K.; Ng, A.L.; Brereton, I.M.; Guddat, L.W.; de Jersey, J. (2006). Lead compounds for antimalarial chemotherapy: purine base analogs discriminate between human and *P. falciparum* 6-oxopurine phosphoribosyltransferases. *J Med Chem*, 49, 7479-86.

Keough, D.T.; Hocková, D.; Holý, A.; Naesens, L.M.; Skinner-Adams, T.S.; Jersey, J.; Guddat, L.W. (2009). Inhibition of hypoxanthine-guanine phosphoribosyltransferase by acyclic nucleoside phosphonates: a new class of antimalarial therapeutics. *J Med Chem,* 52, 4391-9.

Keough, D.T.; Hocková, D.; Krecmerová, M.; Cesnek, M.; Holý, A.; Naesens, L.; Brereton, I.M.; Winzor, D.J.; de Jersey, J.; Guddat, L.W. (2010). *Plasmodium vivax* hypoxanthine-guanine phosphoribosyltransferase: a target for anti-malarial chemotherapy. *Mol Biochem Parasitol,* 173, 165-9.

Lesch, M.; Nyhan, W.L. (1964). A familial disorder of uric acid metabolism and central nervous system function. *Am J Med*, 36, 561-70.

Li, C.M.; Tyler, P.C.; Furneaux, R.H.; Kicska, G.; Xu, Y.; Grubmeyer, C.; Girvin, M.E.; Schramm, V.L. (1999). Transition-state analogs as inhibitors of human and malarial hypoxanthine-guanine phosphoribosyltransferases. *Nat Struct Biol,* 6, 582-7.

Lindsay, S.W.; Martens, W.J. (1998). Malaria in the African highlands: past, present and future. *Bull World Health Organ,* 76, 33-45.

López, J.M. (2008). Is ZMP the toxic metabolite in Lesch-Nyhan disease? *Med Hypotheses,* 71, 657-63.

Madrid, D.C.; Ting, L.M.; Waller, K.L.; Schramm, V.L.; Kim, K. (2008). *Plasmodium falciparum* purine nucleoside phosphorylase is critical for viability of malaria parasites. *J Biol Chem,* 283, 35899-907.

Mendis, K.; Sina, B.J.; Marchesini, P.; Carter, R. (2001). The neglected burden of *Plasmodium vivax* malaria. *Am J Trop Med Hyg*, 64, 97-106.

Mendz, G.L.; Shepley, A.J.; Hazell, S.L.; Smith, M.A. (1997). Purine metabolism and the microaerophily of *Helicobacter pylori. Arch Microbiol,* 168, 448-56.

Musick, W.D. (1981). Structural features of the phosphoribosyltransferases and their relationship to the human deficiency disorders of purine and pyrimidine metabolism. *CRC Crit Rev Biochem*, 11, 1-34.

National Institute Of Allergy And Infectious Diseases (2001). Gene Sequence Of Deadly *E. coli* Reveals Surprisingly Dynamic Genome. *ScienceDaily*. Retrieved June 19, 2010, from http://www.sciencedaily.com /releases/2001/01/010125082330.htm

Neuhard, J. and Nygaard, P. (1987). Purines and pyrimidines. In *Escherichia coli* and *Salmonella typhimurium*: *Cellular and molecular biology*, vol 1 (eds. F.C. Neihardt, J.L. Ingraham, K. Brooks Low, B. Magasanik, M. Schaechter, and H.E. Umbarger), pp. 445–473. American Society for Microbiology, Washington, D.C.

Parker, M.D.; Hyde, R.J.; Yao, S.Y.; McRobert, L.; Cass, C.E.; Young, J.D.; McConkey, G.A.; Baldwin, S.A. (2000). Identification of a nucleoside/nucleobase transporter from *Plasmodium falciparum*, a novel target for anti-malarial chemotherapy. *Biochem J*, 349, 67-75.

Paterson, D.L.; Bonomo, R.A. (2005). Extended-spectrum beta-lactamases. *Clin Microbiol Rev*, 18, 657-86.

Scapin, G.; Grubmeyer, C.; Sacchettini, J.C. (1994). Crystal structure of orotate phosphoribosyltransferase. *Biochemistry*, 33, 1287-94.

Seegmiller, J.E.; Rosenbloom, F.M.; Kelley, W.N. (1967). Enzyme defect associated with a sex-linked human neurological disorder and excessive purine synthesis. *Science*, 155, 1682-4.

Shi, W.; Li, C.M.; Tyler, P.C.; Furneaux, R.H.; Grubmeyer, C.; Schramm, V.L.; Almo, S.C. (1999). The 2.0 Å structure of human hypoxanthine-guanine phosphoribosyltransferase in complex with a transition-state analog inhibitor. *Nat Struct Biol*, 6, 588-93.

Tabor, S.; Richardson, C.C. (1985). A bacteriophage T7 RNA polymerase/promoter system for controlled exclusive expression of specific genes. *Proc Natl Acad Sci USA*, 82, 1074-8.

Ting, L.M.; Shi, W.; Lewandowicz, A.; Singh, V.; Mwakingwe, A.; Birck, M.R.; Ringia, E.A.; Bench, G.; Madrid, D.C.; Tyler, P.C.; Evans, G.B.; Furneaux, R.H.; Schramm, V.L.; Kim, K. (2005). Targeting a novel *Plasmodium falciparum* purine recycling pathway with specific immucillins. *J Biol Chem*, 280, 9547-54.

Ullman, B.; Carter, D. (1997). Molecular and biochemical studies on the hypoxanthine-guanine phosphoribosyltransferases of the pathogenic haemoflagellates. *Int J Parasitol*, 27, 203-13.

Vos, S.; de Jersey, J.; Martin, J.L. (1996). Crystallization and preliminary X-ray crystallographic studies of *Escherichia coli* xanthine phosphoribosyltransferase. *J Struct Biol,* 116, 330-4.

Vos, S.; de Jersey, J.; Martin, J.L. (1997). Crystal structure of *Escherichia coli* xanthine phosphoribosyltransferase. *Biochemistry*, 36, 4125-34.

Vos, S.; Parry, R.J.; Burns, M.R.; de Jersey, J.; Martin, J.L. (1998). Structures of free and complexed forms of *Escherichia coli* xanthine-guanine phosphoribosyltransferase. *J Mol Biol*, 282, 875-89.

Walsh, C.J.; Sherman, I.W. (1968). Purine and pyrimidine synthesis by the avian malaria parasite, *Plasmodium lophurae*. *J Protozool*, 15, 763-70.

Wong, C.S.; Jelacic, S.; Habeeb, R.L.; Watkins, S.L.; Tarr, P.I. (2000). The risk of the hemolytic-uremic syndrome after antibiotic treatment of *Escherichia coli* O157:H7 infections. *N Engl J Med*, 342, 1930-6.

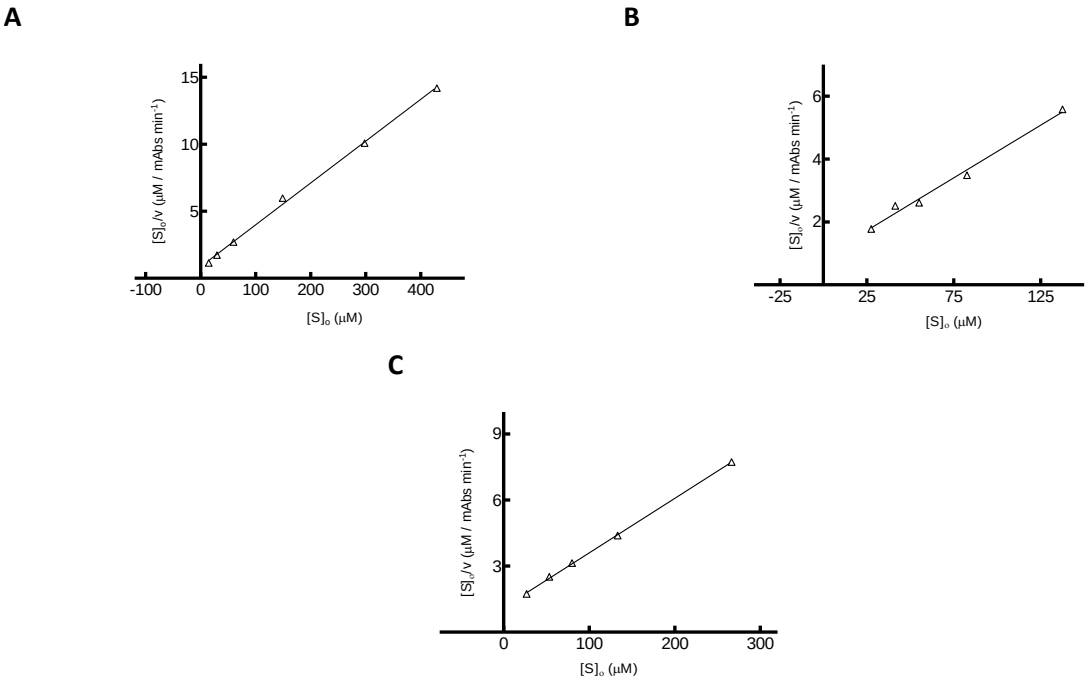

Figure 1. Hanes-Woolf plots for the determination of K_m values for *P*Rib-*PP*. The concentration of *P*Rib-*PP* was varied and the concentration of guanine was fixed at 50 µM. **A** Wild type *E. coli* XGPRT **B** Loop-out *E. coli* XGPRT **C** *E. coli* HPRT.

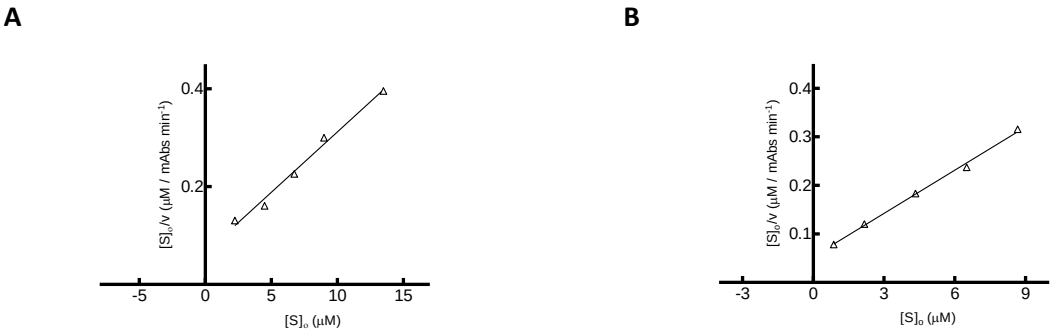

Figure 2. Hanes-Woolf plots for the determination of K_m values for guanine. The concentration of guanine was varied and the concentration of *P*Rib-*PP* was fixed at 400 µM. **A** Wild type *E. coli* XGPRT **B** Loop-out *E. coli* XGPRT.

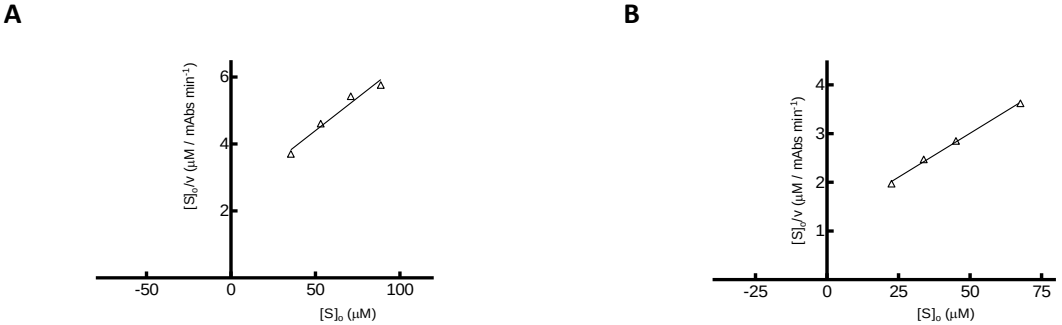

Figure 3. Hanes-Woolf plots for the determination of K_m values for hypoxanthine and xanthine for loop-out *E. coli* XGPRT. The concentration of hypoxanthine and xanthine were varied and the concentration of *P*Rib-*PP* was fixed at 460 µM. **A** Determination of K_m value for hypoxanthine **B** Determination of K_m value for xanthine.

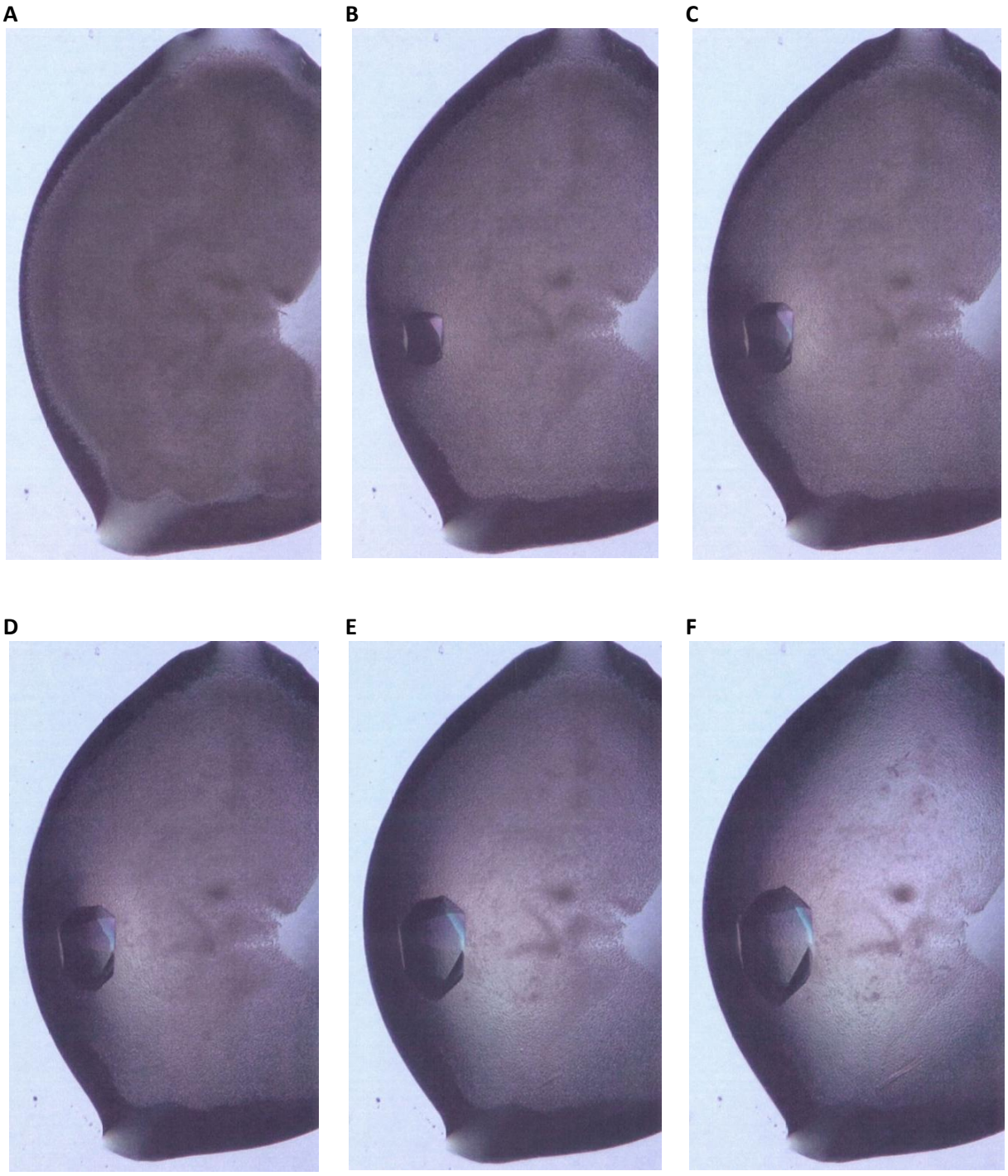

Figure 1. Photographs of a DR3876-bound *E. coli* XGPRT crystal at various moments in time. All pictures are taken automatically from the same hanging drop at prescribed times. Crystallization conditions were 20% (w/v) PEG 3350, 8% tacsimate, pH 6.0. **A** Picture taken directly after setup of the screening plate. **B** Picture taken after 24 hours. **C** After 36 hours. **D** After 60 hours. **E** After 108 hours. Crystal has almost reached maximum size. **F** After 14 days and 12 hours. The size of the crystal is unchanged and the quality of the crystal has not deteriorated.

MASTER'S THESIS PART 2: RESEARCH PROPOSAL

ANTIBACTERIAL AND ANTIMALARIAL ACTIVITY

OF THE ACYCLIC NUCLEOSIDE PHOSPONATE DR3876

1. INTRODUCTION AND BACKGROUND

The 6-oxopurine phosphoribosyltransferases (PRTases) are key enzymes in the purine salvage pathway and synthesize the 6-oxopurine nucleoside monophosphates (GMP, IMP and XMP) essential for RNA and DNA production. These enzymes all contain a highly flexible loop. It has been proposed that this loop closes over the active site during catalysis to shield the transition state in the active site from solvent (*Scapin et al., 1994*).

Protozoan parasites, such as *P. falciparum* and *P. vivax*, are purine auxotroph and their HG(X)PRT enzymes provide the only metabolic pathway to produce the 6-oxopurine nucleoside monophosphates and are, therefore, essential for their growth and survival. For that reason, the 6-oxopurine PRTases have been suggested as promising drug targets (*Walsh & Sherman, 1968*), for the development of anti-malarial drugs. Although bacteria are able to synthesize purine nucleotides *de novo*, 6-oxopurine PRTases have also been described as potential antibacterial drug targets. This has been the case for *H. pylori* (*Duckworth et al., 2006*), where XGPRT is considered to be essential for the survival of the bacterium (*Chalker et al., 2001*), presumably because of an unknown additional function and *M. tuberculosis* (*Biazus et al., 2009*), as part of combination therapy. Furthermore, *E. coli* has the ability to quickly acquire drug resistance (*Paterson & Bonomo, 2005*; *National Institute Of Allergy And Infectious Diseases, 2001*) and a recent study indicates that treatment with known antibiotics does not improve the outcome of the disease, and may in fact significantly increase the chance of developing hemolytic uremic syndrome if infected with the virulent O157:H7 *E. coli* strain (*Wong et al., 2000*). For this reason, antibiotics using different mechanisms of action, such as inhibition of the *E. coli* 6-oxopurine PRTases, could help to suppress the increase of drug resistance and complications in pathogenic *E. coli* strains.

Inhibitors of the 6-oxopurine PRTases can be found in the acyclic nucleoside phosphonates (ANPs), which are structural analogs of the nucleoside 5'-monophosphate products of the reaction catalyzed by the 6-oxopurine PRTases. These compounds inhibit human HGPRT (*Keough et al., 2009*), *Pf*HGXPRT (*Keough et al., 2009*), *Pv*HGPRT (*Keough et al., 2010*), *E. coli* XGPRT (*Keough et al., unpublished*) and *E. coli* HPRT (*Keough et al., unpublished*). The ANPs in general have favorable pharmacokinetic properties and have relatively low cytotoxicity in mammalian cells (*Keough et al., 2009*).

2. AIMS

1) As *in vitro* inhibition studies of the ANPs resulted in a good inhibitor of *E. coli* XGPRT, namely DR3876 (K_i = 0.23 ± 0.03 µM), it is highly interesting to examine this inhibitor's antibacterial activity. Knock-out of *de novo* purine synthesis in *E. coli* (*Benson et al., 1970*) in combination with inhibition of its 6-oxopurine salvage enzymes, has been proposed as a strategy to suppress the increase of drug resistance and complications in pathogenic *E. coli* strains (part 1, section 1.4). Therefore, the following question is asked:

To what extent is DR3876 able to cross the *E. coli* bacterial cell wall and inhibit bacterial growth?

2) The ANP DR3876 has been originally developed as an antimalarial drug. Results from the experiments to investigate the interactions between DR3876 and the *E. coli* 6-oxopurine salvage enzymes (part 1, section 4) can be used as a template for the study of DR3876 inhibition of *Pf*HGXPRT and *Pv*HGPRT. As DR3876 is a good inhibitor of the bacterial salvage enzymes, inhibition studies of these parasite enzymes are highly advisable. Hence, the following questions are asked:

Is DR3876 a good inhibitor of *Pf*HGXPRT and *Pv*HGPRT? And if so, is DR3876 able to arrest parasitemia in infected erythrocytes in culture?

3. PRELIMINARY RESULTS

Kinetic constants for the natural occurring substrates (*Vos et al., 1997*; *Guddat et al., 2002*; *Keough et al., unpublished results*) as well as K_i values of the nucleoside 5'-monophosphate products of the reaction (*Guddat et al., 2002*; *Keough et al., unpublished results*) have been determined for the three *E. coli* enzymes (wild type XGPRT, loop-out XGPRT and HPRT). Also, K_i values have been determined for these three *E. coli* enzymes for three ANPs DR3876, MK520 and MK455 (part 1, section 4.3). In addition, highly diffracted crystals of DR3876-bound *E. coli* XGPRT have been obtained (part 1, section 4.6). However, inhibition of bacterial growth by this class of inhibitors has not been tested yet.

For *Pf*HGXPRT and *Pv*HGPRT, kinetic constants for the naturally occurring substrates as well as K_i values for a number of ANPs have been determined (*Keough et al., 2009; Keough et al., 2010*). The crystal structure of *Pf*HGXPRT has been solved in the presence of a transition-state analogue inhibitor (*Shi et al., 1999*). This result illustrates the structural properties of the parasite enzyme and the interactions which occur when the inhibitor binds.

In order to inhibit the malarial parasite growth in erythrocytes, the ANP has to permeate through the erythrocyte and parasite membranes. Transport of acyclic nucleoside analogs, such as the antiviral drugs acyclovir en desciclovir, through the human erythrocyte membrane has been examined and was found to occur by nucleobase carriers (*Mahony et al., 1988)* and nonfacilitated diffusion (*Domin et al., 1991*).

Certain ANPs have been shown to inhibit the growth of *P. falciparum* in culture. A previous study showed that (*S*)-9-[3-hydroxy-2-(phosphonomethoxy)propyl] adenine [(*S*)-HPMPA] is toxic to *P. falciparum* with an IC_{50} value of 4 µM (*De Clercq & Holý, 2005*). Another recent study showed that 9-[2-(phosphonomethoxy)ethyl] guanine (PMEG), cyclic-(*S*)-9-[3-hydroxy-2-(phosphonomethoxy)propyl] guanine (cyclic-(*S*)-HPMPG) and cyclic-(*R*)-9-[3-hydroxy-2-(phosphonomethoxy)propyl] guanine (cyclic-(*R*)-HPMPG) inhibit the growth *of P. falciparum* in erythrocyte cultures with IC_{50} values of 14 µM, 1 µM and 46 µM, respectively (*Keough et al., 2009*). These results support the hypothesis that inhibition of *Pf*HGXPRT is responsible for toxicity to the parasite. However, the pharmacokinetic and pharmacologic properties (absorption, distribution, metabolism, excretion) of the ANPs will play an important role for inhibition of the growth of *P. falciparum in vivo*.

4. RESEARCH DESIGN

4.1. ANTIBACTERIAL EFFECTS OF DR3876

4.1.1. Inhibitory effect on bacterial growth

The inhibitory effect of DR3876 on the bacterial growth of *E. coli* O157:H7 cells can be examined in a similar way as a method described by *Wang et al.* (*2002*). The *E. coli* O157:H7 serotype can be grown in a rich medium, such as Lysogeny broth (LB) agar plates. A single colony of the agar plate is inoculated into 10 ml of minimal medium, such as AB medium. The overnight culture is diluted in minimal media until an initial A_{600} of 0.01 is reached. Of these inoculated media, 1 ml is added to a set of sterilized tubes. A dilution of DR3876 (in AB medium) at concentrations ranging from 1×10^{-3} to 1×10^{-10} M is prepared from a stock solution. Next, 20 ml of each dilution (also containing 1 mM of 6-methylpurine, a *de novo* purine synthesis inhibitor) is added to the set of tubes. To the control tube, 20 ml of minimal medium is added. Meropenem, 20 ml in a concentration of 10 mg/ml, is added to a positive control tube.

The tubes are cultured at 37°C with shaking until the control tube reaches an A_{600} of 0.6. Next, the A_{600} values of the remaining tubes are measured and the inhibition percentage of each dilution of DR3876 can be calculated comparing its A_{600} to that of the control tube, which represents 100% bacterial growth. Results are only valid if there is no bacterial growth in the positive control tube.

4.1.2. Inhibition of growth of epithelial cell-invaded bacteria

The next model, which is derived from an invasion assay described by *Xicohtencatl-Cortes et al.* (*2008*), can be used to examine the inhibition of bacterial cell growth after invasion of *E. coli* O157:H7 in human epithelial cells. A variety of cell lines can be used: human polarized colonic (HT-29), nonintestinal (HeLa and HEp-2), and Madin-Darby bovine kidney (MDBK) epithelial cell lines. These cell lines are grown in monolayers in 24-well plates containing Dulbecco's minimal essential medium (DMEM). Cells are grown until at least 80% of the plate is covered by the cells. The wells are incubated with about 1×10^{7} *E. coli* O157:H7 cells, obtained from the overnight culture (section 4.1.1). After incubation, the supernatant is removed and replaced by fresh DMEM. After 6 h, the wells are washed three times with phosphate buffered saline (PBS). To kill residual extracellular bacteria, gentamicin at 100 µg/ml is added to the 24-well plates for 1h.

Next, the wells are washed three times and incubated with dilutions of DR3876 at concentrations from 1 x 10^{-3} to 1 x 10^{-10} M (and 1 mM of 6-methylpurine) for 4 h. Cells in the control well are grown in the absence of ANP. Cells in the positive control well are grown in the presence of meropenem/tigecycline. The cells are then washed three times with PBS, lysed with 1 ml of 0.1% Triton X-100 in PBS, and plated onto LB agar plates with the appropriate antibiotics. The percentage of growth inhibition of epithelial cell-invaded *E. coli* can be calculated as the number of bacteria surviving incubation with DR3876 divided by the total number of bacteria that grow in the absence of the ANP. Results are only valid if there is no bacterial growth in the positive control well.

To ensure reproducibility and validity of the results, experiments are performed in triplicate and at least three times on separate days. The data are expressed as the means of the averages of the results obtained from the experiments performed.

4.2. ANTIMALARIAL EFFECTS OF DR3876

4.2.1. Inhibition of *Pf*HGXPRT and *Pv*HGPRT by DR3876

Prior to determination of the K_i values of DR3876 for *Pf*HGXPRT and *Pv*HGPRT, the K_m value for *P*Rib-*PP* and guanine or hypoxanthine are determined for the two parasite enzymes. Secondly, the concentration of inhibitor that gives good inhibition of the parasite enzymes is determined. These experiments can be carried out using a spectrophotometric assay under the same conditions and protocols as described previously (part 1, section 3.6-3.8).

The K_i values are determined using a spectrophotometric assay with the same extinctions coefficients, wave-lengths and enzyme concentrations as described above (part 1, section 3). K_i values can be determined by Hanes-Woolf plots and calculated using Prism (GraphPad Software, Inc., La Jolla, United States). Also, K_i values can be calculated using the equations $K_{m\,(app)} = K_m \mathbf{(}1+ ([I]/K_i)\mathbf{)}$ and $v_0 = \mathbf{(}V_{max}\,[S]_0\mathbf{)} / \mathbf{(}K_m + [S]_0\mathbf{)}$.

4.2.2. Effect of DR3876 on *P. falciparum* in cell culture

4.2.2.1. Culture of selected *P. falciparum* isolate

A culture of a laboratory-adapted *P. falciparum* isolate can be maintained in modified candle jars as described by *Trager & Jensen* (*1976*). The next part of this method involves a series of

important requirements for long-term experiments such as (1) erythrocytes in a shallow stationary layer covered by a shallow layer of medium that flows slowly and continuously over the settled cells, (2) an atmosphere of relatively high CO_2 and low O_2 and (3) a method for change of medium with minimal disturbance of the erythrocytes. This technique is developed specifically for *P. falciparum,* but not *P. vivax*.

A dilution of DR3876 at concentrations ranging from 1×10^{-4} to 1×10^{-10} M is prepared from a stock solution. 100 µl of each dilution is added in wells of sterile flat-bottom 96-well microtitre plates in duplicate (*Hamza et al., 2003*). Parasite cultures are diluted to a standard of 2% parasitemia (*i.e.* the percentage of parasite-infected erythrocytes) and 1% haematocrit (*i.e.* the percentage of blood volume that is occupied by erythrocytes). The diluted parasite cultures are then added (100 µl) to the wells (total well volume of 200 µl). The control well consists of 100 µl of diluted parasite culture and 100 µl of isotone water. PMEG (100 µl of 0.3 mM PMEG) is added to 100 µl of diluted parasite culture in the positive control well.

The *in vitro* efficacy of DR3876 against the specific *P. falciparum* isolate is determined by assessing parasitemia after 48h hours of incubation. Results are only valid if there is no parasitemia in the positive control well. Assessment of parasitemia can be performed in a variety of ways, such as Giemsa staining and flow cytometry.

4.2.2.2. Giemsa staining and light microscopy

Blood smears are prepared from each well culture and stained with Giemsa (*Giemsa, 1904*). Giemsa stain is a classical blood film stain and is the stain of choice for demonstrating the presence of parasites in blood smears. This type of stain is specific for the phosphate groups of DNA and binds strongly to AT-rich regions of DNA and can be used for histo-pathological diagnosis of malaria.

A number of procedures is described for the staining of thin blood smears with Giemsa (*Barcia, 2007; Laboratory Identification of Parasites of Public Health concern, Diagnostic procedures, Blood specimen bench aids, Staining for malaria parasites, 2009*). First, a thin film of blood is fixed on a slide and the thin film is dried by air at room temperature. The film is dipped in absolute methanol or, alternatively, a few drops of absolute methanol are put on the slide with a pipette. After 30 seconds to 1 minute, the slide is washed in tap water and submerged

with working stain solution (2.5 %). The slide is placed in the solution, face downwards on two glass rods. The working stain solution (40 ml distilled buffered water + 1 ml Giemsa stain stock solution + 20 µl of 5 % Triton-X 100 solution) must be newly prepared each time. The Giemsa stain stock solution can be prepared by adding 30 ml of glass beads, 270 ml of absolute acetone-free methanol, 3 g of certified Giemsa stain powder and 140 ml of glycerol to a brown glass bottle. The bottle is shaken for 30-60 minutes every day, for at least 14 days. This stock solution is stable at room temperature indefinitely, if free from moisture. The slide is stained for 45-60 minutes. Afterwards, the slide is washed again with tap water to float off the stain excess and to prevent deposition of precipitate on to the film. Slides are placed upright to dry by air at room temperature. An example of Giemsa staining of *P. falciparum* infected erythrocytes is shown in Figure 4.1.

Alternatively, the smears can be stained for shorter times in more concentrated stains. One alternative is 10 minutes in 10 % Giemsa working stain solution; the shorter stains yield faster results, but use more stain and might be of less predictable quality.

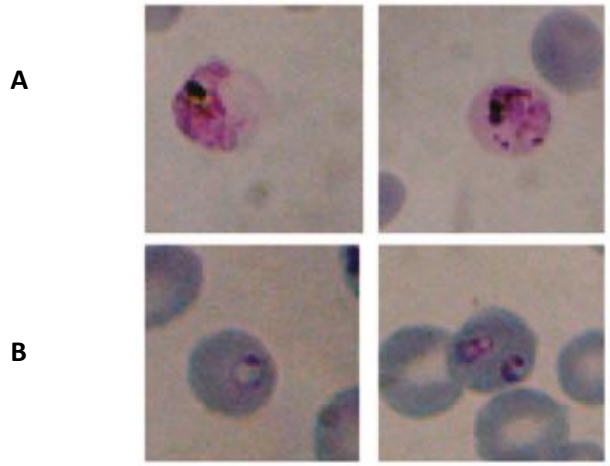

Figure 4.1. Giemsa staining of erythrocytes. In the presence of Giemsa, erythrocytes stain light pink/purple, while parasites stain dark blue/purple/pink. **A** *P. falciparum* parasites grown in the presence of PMEG show extensive cellular damage and decreased development. **B** Parasites grown in the absence of PMEG illustrate no damage or inhibition of development (*Keough et al., 2009*).

Blood smears can now be examined using light microscopy and the level of parasitemia can be determined. To ensure reproducibility and avoid wrong interpretation of the results, it is advised to examine the tail end of the slide where the erythrocytes are separated into a one-cell-layer.

4.2.2.3. Flow cytometry

An alternative method of parasite detection and determination of parasitemia is flow cytometry. Flow cytometry is a high throughput technique for the analysis (counting and examination) of small individual particles, such as cells (*Davis, 2001*). The cells are suspended in a flow stream that passes through a capillary tube. A technique called hydrodynamic focusing ensures that the cells enter the capillary tube one by one. This technique involves a sheath fluid that is being pumped in the capillary tube, while the sample solution is injected as a core stream into the middle of the sheath flow. This sheath flow has a higher velocity and forms a wall around the sample solution and thereby focuses the cells in the sample solution. Light from one or more excitation light sources, typically laser beams, is directed at each individual cell as it passes through (*Ibrahim & van den Engh, 2007*). Interaction between the laser light and each cell results in specific scattering of light and activation of fluorescent dyes, such as SYBR Green. SYBR Green is an asymmetrical fluorescent dye that binds to double stranded DNA with great specificity (*Zabzdyr & Lillard, 2001*). It is substantially more sensitive than ethidium bromide, another commonly used stain for the visualization of DNA. SYBR Green easily penetrates cells and the resulting complex with DNA absorbs light with an λ_{max} of 488 nm and emits light at an λ_{max} of 522 nm (*Zipper et al., 2004*). Scattered light and emitted fluorescent light are then detected and measured with photomultipliers. Thousands of particles can be analyzed per second. The general structure of a flow cytometer is shown in Figure 4.2.

Since human erythrocytes are non-nucleated cells, they lack DNA and RNA. Uninfected erythrocytes will therefore show no binding of SYBR Green. Infected cells however, will exhibit a high amount of emitted fluorescent light, due to the high amount of parasite DNA bound to SYBR Green. This distinction in emitted fluorescent light is the key principle to distinguish between infected and uninfected erythrocytes and to determine the level of parasitemia.

A flow cytometry-based method is described by *Bei et al. (2010)* and involves centrifugation (1200 rpm, 5 min) of the culture after 48h. The pellet is then washed twice in 100 µl PBS + 0.5% bovine serum albumin (BSA) + 0.02% sodium azide. Cells are incubated with 75 µl of a 1:1000 SYBR Green I solution for 20 min at 25°C. Afterwards, cells are washed in PBS + 0.5% BSA + 0.02% sodium azide and resuspended in PBS. Data are collected by a flow cytometer.

It is necessary to carry out a blank sample with unstained, uninfected erythrocytes to account for erythrocyte autofluorescence.

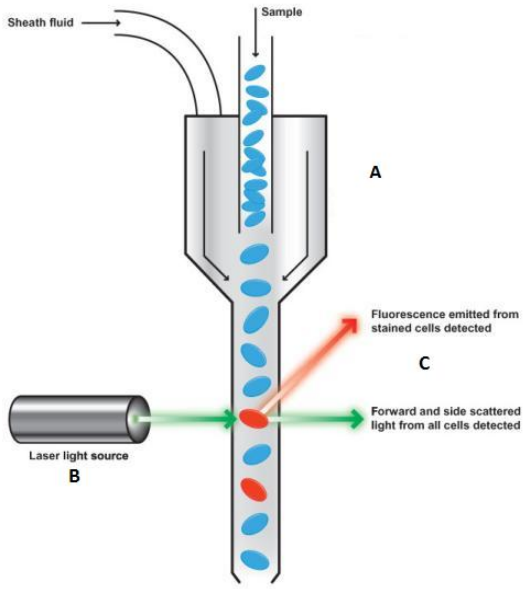

Figure 4.2. Flow cytometer. A flow cytometer generally consists of 5 main components: (A) a flow cell with sheath fluid to align the cells so that they pass single file through the laser beam, (B) a measuring system which commonly consists of a laser light source, (C) a detector used for the detection of scattered light and emitted fluorescence signals. The amplification system and computer system for the analysis of the signals are not shown in the figure *(Sony Insider, 2010).*

This method yields results that are highly comparable to light microscopy (*Bei et al., 2010*) and has the advantage to be less time-intensive and less subjective. However, it is reported that sensitivity can be up to 10 times less than the Giemsa staining-light microscopy method, caused by a high level of background noise, caused by stained RNA in reticulocytes (*Hänscheid, 1999*).

4.2.2.4. Results and IC_{50} determination

Giemsa staining of blood smears in combination with light microscopy is the currently preferred method and leads to the most precise and accurate results (*Hänscheid, 1999*). The percentage growth inhibition of each dilution can be calculated from the comparison to untreated controls. The concentrations of DR3876 required to inhibit parasite growth by 50% (IC_{50}) can be determined by linear interpolation.

As a control for this experiment, duplicates of the examined wells can be investigated in the event of a problem during the examination process and/or in case of the need of confirmation of previous results.

5. PERSPECTIVE

The main objective in this research proposal is to investigate the antibacterial and antimalarial efficacy of a specific ANP, i.e., DR3876. This is a first step in investigating the potential usefulness of the well-known class of ANP drugs on completely new targets of medical interest, namely *E. coli* and *P. falciparum*.

In case that the ANP DR3876 is indeed shown to have antibacterial and/or antiplasmodial activity, this could broaden the horizon for treatment of numerous infections. Especially important in this point of view, is that the ANPs could form a potential answer for the current problems of dealing with the expansion of therapy resistant pathogens. This research can then be seen as a stepping stone for the enhancement of existing ANPs and the discovery of new and more effective molecules.

6. REFERENCES

Barcia, J.J. (2007). The Giemsa stain: its history and applications. *Int J Surg Pathol*, 15, 292-296.

Bei, A.K.; Desimone, T.M.; Badiane, A.S.; Ahouidi, A.D.; Dieye, T.; Ndiaye, D.; Sarr, O.; Ndir, O.; Mboup, S.; Duraisingh, M.T. (2010). A flow cytometry-based assay for measuring invasion of red blood cells by *Plasmodium falciparum*. *Am J Hematol*, 85, 234-7.

Benson, C.E.; Love, S.H.; Remy, C.N. (1970). Inhibition of *de novo* purine biosynthesis and interconversion by 6-methylpurine in *Escherichia coli. J Bacteriol,* 101, 872-80.

Biazus, G.; Schneider, C.Z.; Palma, M.S.; Basso, L.A.; Santos, D.S. (2009). Hypoxanthine-guanine phosphoribosyltransferase from *Mycobacterium tuberculosis* H37Rv: cloning, expression, and biochemical characterization. *Protein Expr Purif*, 66, 185-90.

Chalker, A.F.; Minehart, H.W.; Hughes, N.J.; Koretke, K.K.; Lonetto, M.A.; Brinkman, K.K.; Warren, P.V.; Lupas, A.; Stanhope, M.J.; Brown, J.R.; Hoffman, P.S. (2001). Systematic identification of selective essential genes in *Helicobacter pylori* by genome prioritization and allelic replacement mutagenesis. *J Bacteriol,* 183, 1259-68.

Davis, B.H. (2001). Diagnostic utility of red cell flow cytometric analysis. *Clin Lab Med*, 21, 829-40.

De Clercq, E.; Holý, A. (2005). Acyclic nucleoside phosphonates: a key class of antiviral drugs. *Nat Rev Drug Discov*, 4, 928-40.

Domin, B.A.; Mahony, W.B.; Zimmerman, T.P. (1991). Desciclovir permeation of the human erythrocyte membrane by nonfacilitated diffusion. *Biochem Pharmacol*, 42, 147-52.

Duckworth, M.; Ménard, A.; Megraud, F.; Mendz, G.L. (2006). Bioinformatic analysis of *Helicobacter pylori* XGPRTase: a potential therapeutic target. *Helicobacter*, 11, 287-95.

Giemsa, G. (1904). Eine vereinfachung und vervollkommnung meiner methylenazur-methlyenblau-eosin-farbemethode zur erzielung der Romanowsky-Nocht'schen chromatinfarbung. Zentabl. Bakteriol. Parasitenkd. Infectkrankh.37:308.

Guddat, L.W.; Vos, S.; Martin, J.L.; Keough, D.T.; de Jersey, J. (2002). Crystal structures of free, IMP-, and GMP-bound *Escherichia coli* hypoxanthine phosphoribosyltransferase. *Protein Sci*, 11, 1626-38.

Hamzah, J.; Skinner-Adams, T.S.; Davis, T.M. (2003). *In vitro* antimalarial activity of retinoids and the influence of selective retinoic acid receptor antagonists. *Acta Trop*, 87, 345-53.

Hänscheid, T. (1999). Diagnosis of malaria: a review of alternatives to conventional microscopy. *Clin Lab Haematol*, 21, 235-45.

Ibrahim, S.F.; van den Engh, (2007). Flow cytometry and cell sorting. *Advances in biochemical engineering/biotechnology*, 106, 19-39.

Keough, D.T.; Hocková, D.; Holý, A.; Naesens, L.M.; Skinner-Adams, T.S.; Jersey, J.; Guddat, L.W. (2009). Inhibition of hypoxanthine-guanine phosphoribosyltransferase by acyclic nucleoside phosphonates: a new class of antimalarial therapeutics. *J Med Chem,* 52, 4391-9.

Keough, D.T.; Hocková, D.; Krecmerová, M.; Cesnek, M.; Holý, A.; Naesens, L.; Brereton, I.M.; Winzor, D.J.; de Jersey, J.; Guddat, L.W. (2010). *Plasmodium vivax* hypoxanthine-guanine phosphoribosyltransferase: a target for anti-malarial chemotherapy. *Mol Biochem Parasitol,* 173, 165-9.

Laboratory Identification of Parasites of Public Health concern, Diagnostic procedures, Blood specimen bench aids, Staining for malaria parasites. (2009). Retrieved September 6, 2010, from www.dpd.cdc.gov/dpdx/html/PDF_Files/malaria_staining_benchaid.pdf 2009

Mahony, W.B.; Domin, B.A.; McConnell, R.T.; Zimmerman, T.P. (1988). Acyclovir transport into human erythrocytes. *J Biol Chem*, 263, 9285-91.

National Institute Of Allergy And Infectious Diseases (2001). Gene Sequence Of Deadly *E. coli* Reveals Surprisingly Dynamic Genome. *ScienceDaily*. Retrieved June 19, 2010, from http://www.sciencedaily.com /releases/2001/01/010125082330.htm

Paterson, D.L.; Bonomo, R.A. (2005). Extended-spectrum beta-lactamases: a clinical update. *Clin Microbiol Rev*; 18, 657-86.

Scapin, G.; Grubmeyer, C.; Sacchettini, J.C. (1994). Crystal structure of orotate phosphoribosyltransferase. *Biochemistry*, 33, 1287-94.

Shi, W.; Li, C.M.; Tyler, P.C.; Furneaux, R.H.; Grubmeyer, C.; Schramm, V.L.; Almo, S.C. (1999). The 2.0 Å structure of human hypoxanthine-guanine phosphoribosyltransferase in complex with a transition-state analog inhibitor. *Nat Struct Biol*, 6, 588-93.

Sony Insider, Sony Acquires iCyt And Officially Enters Flow Cytometry Business. Retrieved October 11, 2010, from http://www.sonyinsider.com/2010/02/12/sony-acquires-icyt-and-officially-enters-flow-cytometry-business/

Trager, W.; Jensen, J.B. (1976). Human malaria parasites in continuous culture. *Science*, 193, 673-5.

Vos, S.; de Jersey, J.; Martin, J.L. (1997). Crystal structure of *Escherichia coli* xanthine phosphoribosyltransferase. *Biochemistry*, 36, 4125-34.

Walsh, C.J.; Sherman, I.W. (1968). Purine and pyrimidine synthesis by the avian malaria parasite, *Plasmodium lophurae*. *J Protozool*, 15, 763-70.

Wang, J.; Su, C.; Neuhard, J.; Eriksson, S. (2000). Expression of human mitochondrial thymidine kinase in *Escherichia coli*: correlation between the enzymatic activity of pyrimidine nucleoside analogues and their inhibitory effect on bacterial growth. *Biochem Pharmacol*, 59, 1583-8.

Wong, C.S.; Jelacic, S.; Habeeb, R.L.; Watkins, S.L.; Tarr, P.I. (2000). The risk of the hemolytic-uremic syndrome after antibiotic treatment of *Escherichia coli* O157:H7 infections. *N Engl J Med*, 342, 1930-6.

Xicohtencatl-Cortes, J.; Monteiro-Neto, V.; Saldaña, Z.; Ledesma, M.A.; Puente, J.L.; Girón, J.A. (2009). The type 4 pili of enterohemorrhagic *Escherichia coli* O157:H7 are multipurpose structures with pathogenic attributes. *J Bacteriol,* 191, 411-21.

Zabzdyr, J.L.; Lillard, S.J. (2001). UV- and visible-excited fluorescence of nucleic acids separated by capillary electrophoresis. *J Chromatogr A*, 911, 269-76.

Zipper, H.; Brunner, H.; Bernhagen, J.; Vitzthum, F. (2004). Investigations on DNA intercalation and surface binding by SYBR Green I, its structure determination and methodological implications. *Nucleic Acids Res*, 32, 103.